Available online at www.sciencedirect.com
ScienceDirect
Geochimica et Cosmochimica Acta 74 (2010) 6517–6540
Geochimica et Cosmochimica Acta
www.elsevier.com/locate/gca

Assessment of grain-scale homogeneity and equilibration of carbon and oxygen isotope compositions of minerals in carbonate-bearing metamorphic rocks by ion microprobe

John M. Ferry [a,*], Takayuki Ushikubo [b], Noriko T. Kita [b], John W. Valley [b]

[a] Department of Earth and Planetary Sciences, Johns Hopkins University, Baltimore, MD 21218, USA
[b] WiscSIMS, Department of Geoscience, University of Wisconsin, Madison, WI 53706, USA

Received 25 January 2010; accepted in revised form 11 August 2010

Abstract

Nineteen samples of metamorphosed carbonate-bearing rocks were analyzed for carbon and oxygen isotope ratios by ion microprobe with a ~5–15 μm spot, three from a regional terrain and 16 from five different contact aureoles. Contact metamorphic rocks further represent four groups: calc-silicate marble and hornfels (6), brucite marble (2), samples that contain a reaction front (4), and samples with a pervasive distribution of reactants and products of a decarbonation reaction (4). The average spot-to-spot reproducibility of standard calcite analyses is ±0.37‰ (2 standard deviations, SD) for $\delta^{18}O$ and ±0.71‰ for $\delta^{13}C$. Ten or more measurements of a mineral in a sample that has uniform isotope composition within error of measurement can routinely return a weighted mean with a 95% confidence interval of 0.09–0.16‰ for $\delta^{18}O$ and 0.10–0.29‰ for $\delta^{13}C$. Using a difference of >6SD as the criterion, only four of 19 analyzed samples exhibit significant intracrystalline and/or intercrystalline inhomogeneity in $\delta^{13}C$ at the 100–500 μm scale, with differences within individual grains up to 3.7‰. Measurements are consistent with carbon isotope exchange equilibrium between calcite and dolomite in five of six analyzed samples at the same scale. Because of relatively slow carbon isotope diffusion in calcite and dolomite, differences in $\delta^{13}C$ can survive intracrystalline homogenization by diffusion during cooling after peak metamorphism and likely represent the effects of prograde decarbonation and infiltration. All but 2 of 11 analyzed samples exhibit intracrystalline differences in $\delta^{18}O$ (up to 9.4‰), intercrystalline inhomogeneity in $\delta^{18}O$ (up to 12.5‰), and/or disequilibrium oxygen isotope fractionations among calcite–dolomite, calcite–quartz, and calcite–forsterite pairs at the 100–500 μm scale. Inhomogeneities in $\delta^{18}O$ and $\delta^{13}C$ are poorly correlated with only a single mineral (dolomite) in a single sample exhibiting both. Because of relatively rapid oxygen isotope diffusion in calcite, intracrystalline inhomogeneities in $\delta^{18}O$ likely represent partial equilibration between calcite and fluid during retrograde metamorphism. Calcite is in oxygen isotope exchange equilibrium with forsterite in one of four analyzed samples, in equilibrium with dolomite in none of six analyzed samples, and in equilibrium with quartz in neither of two analyzed samples. There are no samples of contact metamorphic rock with analyzed reactants and products of an arrested metamorphic reaction that are in oxygen isotope equilibrium with each other. The degree of departure from equilibrium in analyzed samples is variable and is often related, at least in part, to alteration of $\delta^{18}O$ of calcite during retrograde fluid–rock reaction. In situ sub-grain-scale carbon and oxygen isotope analyses of minerals are advisable in the common applications of stable isotope geochemistry to metamorphic petrology. Correlation of sub-mm scale stable isotope data with imaging will lead to improved understanding of reaction kinetics, reactive fluid flow, and thermal histories during metamorphism.

* Corresponding author. Tel.: +1 410 516 8121; fax: +1 410 516 7933.
E-mail address: jferry@jhu.edu (J.M. Ferry).

0016-7037/$ - see front matter © 2010 Elsevier Ltd. All rights reserved.
doi:10.1016/j.gca.2010.08.039

1. INTRODUCTION

The carbon and oxygen isotope compositions of minerals in metamorphic rocks bear directly on the understanding of the process of metamorphism (e.g., reviews by Valley (1986, 2001), Nabelek (1991), Bowman (1998), Baumgartner and Valley (2001)). Many investigations assume that mineral grains are uniform in their isotope composition and that measured compositions represent isotope exchange equilibrium among minerals at the thermal peak of metamorphism. These assumptions have been a practical necessity for most studies because conventional sampling of material for isotope analysis, even by microdrilling, excavates many grains from metamorphic rocks with normal grain size. Nevertheless, a continuing concern in the study of the isotopic composition of metamorphic rocks is whether isotope zoning in metamorphic minerals and grain-to-grain variations in isotope composition may be common at spatial scales <1 mm due to diffusion or fast pathways for intercrystalline exchange (Valley, 2001). Small scale, especially intracrystalline, variability in isotope composition would call into question conclusions reached in studies that used conventional sampling techniques and that assumed such variability did not exist.

Carbon and oxygen isotope zonation in metamorphic minerals and grain-to-grain variations in $\delta^{13}C$ and $\delta^{18}O$, however, are known facts (Wada, 1988; Chamberlain and Conrad, 1991, 1993; Valley and Graham, 1991, 1993; Kohn et al., 1993; Young and Rumble, 1993; Jamtveit and Hervig, 1994; Eiler et al., 1995a,b; Graham et al., 1998; Lewis et al., 1998; Satish-Kumar et al., 1998; Wada et al., 1998; Page et al., 2007, 2010; Bowman et al., 2009; Lancaster et al., 2009). A systematic survey of the extent of grain-scale carbon and oxygen isotope heterogeneity in metamorphic rocks, however, has waited for instrumentation that is capable of rapid, accurate, high-precision measurements of $\delta^{13}C$ and $\delta^{18}O$ at spatial scales smaller than normal grain size. The instrumentation and analytical techniques have now been developed (Kita et al., 2009; Valley and Kita, 2009). Accordingly, we report the first systematic assessment of the degree to which (a) carbonate minerals are isotopically zoned, (b) there is grain-to-grain variability of $\delta^{13}C$ and $\delta^{18}O$, and (c) different minerals attain and preserve isotope exchange equilibrium at the grain-size scale in a suite of representative regional and contact metamorphic rocks.

2. SCOPE OF THE INVESTIGATION

The investigation focused on calcite and dolomite in metamorphosed carbonate-bearing rocks to evaluate intracrystalline and intercrystalline variability of both $\delta^{13}C$ and $\delta^{18}O$. Initially, however, the study emphasized carbon isotopes because two kinds of evidence indicate that intracrystalline and intercrystalline heterogeneities in $\delta^{13}C$ ought to develop and be preserved during metamorphism more readily than heterogeneities in $\delta^{18}O$. The first is experimental. The diffusivity of carbon in calcite is 3–4 orders of magnitude smaller than the diffusivity of oxygen in calcite under "wet" conditions at representative temperatures of metamorphism, 400–700 °C (Farver, 1994; Labotka et al., 2000). Accordingly, as is documented in Section 7.3, calcite is more likely to develop and preserve intracrystalline and intercrystalline variations in $\delta^{13}C$ than in $\delta^{18}O$ during both regional and contact metamorphism.

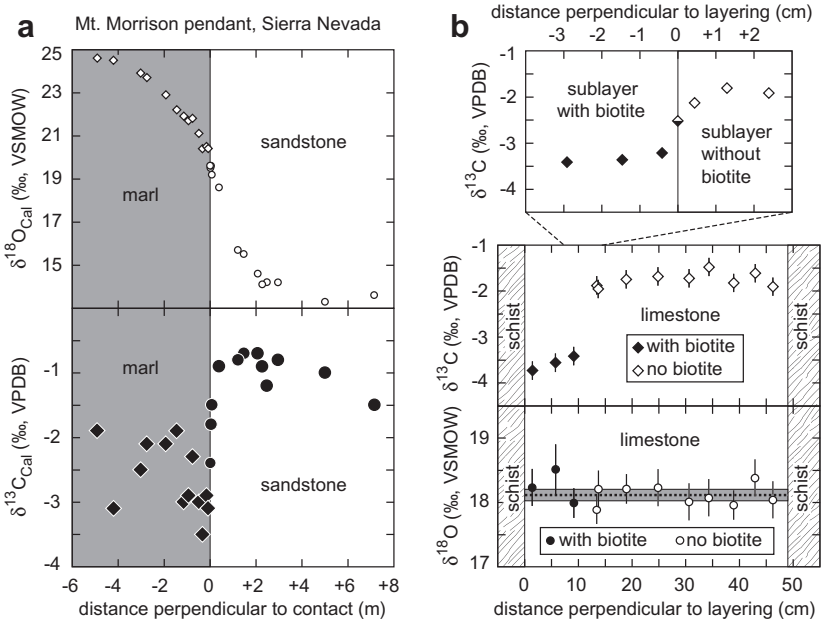

Fig. 1. Profiles in $\delta^{18}O$ and $\delta^{13}C$ across lithologic layering. The error bars or the size of the symbols approximately represent ±2SD uncertainties. (a) Profile across a marl–sandstone contact in the Mt. Morrison pendant, Sierra Nevada, California, USA. Data are from Ferry et al. (2001). (b) Profile across a limestone layer in the Waits River Formation, Vermont, USA. The dashed horizontal line is the weighted mean $\delta^{18}O$, and the gray band is the 95% confidence interval. Data are from Penniston-Dorland and Ferry (2006) supplemented by new measurements from this study (top panel). The much larger intercrystalline exchange distance for $\delta^{18}O$ than for $\delta^{13}C$ is empirical evidence for limited intracrystalline diffusion of carbon isotopes.

The second kind of evidence is empirical. As one example from a contact aureole, a profile in $\delta^{18}O$ of calcite across a marl–sandstone contact in the Mt. Morrison pendant, Sierra Nevada (Fig. 1a), is smooth and implies intercrystalline oxygen isotope exchange over ~7 m during contact metamorphism. Reversals in $\delta^{13}C$ along the same profile, on the other hand, limit intercrystalline carbon isotope exchange to a distance of no more than ~0.3 m, smaller by a factor of at least ~23. As a second example from a regional metamorphic terrain, the $\delta^{18}O$ of carbonate across a 50-cm thick micaceous limestone layer from the Waits River Formation, eastern Vermont, is uniform within error of measurement, implying intercrystalline oxygen isotope exchange over at least 50 cm during regional metamorphism (Fig. 1b). In contrast, there is a steep gradient in $\delta^{13}C$ along the same traverse between biotite-bearing and biotite-free sublayers that sets a limit for intercrystalline carbon isotope exchange of no more than 1–2 cm, smaller by a factor of at least 25. Considering the mole fraction of CO_2 (X_{CO_2}) in fluid during metamorphism (Ferry, 1994; Ferry et al., 2001), Eq. (1) of Bickle et al. (1997) predicts that the intercrystalline exchange distance for oxygen isotopes should be no more than twice that of carbon isotopes along the two traverses if local mineral–fluid equilibrium is maintained. The much smaller than predicted scale of carbon isotope exchange along both traverses implies departures from both intercrystalline and intracrystalline carbon isotope equilibrium (caused by slow carbon isotope diffusion in carbonate minerals) on the time scales of metamorphism, and suggests that small-scale heterogeneity of $\delta^{13}C$ should be more likely than small-scale heterogeneity of $\delta^{18}O$ during both regional and contact metamorphism.

3. SAMPLE SELECTION AND DESCRIPTION

Nineteen samples were selected for study (Table 1). Five criteria were used for sample selection. First, all samples contain carbonate so that the behavior of both carbon and oxygen isotopes could be evaluated. Calcite occurs in all samples, and dolomite occurs additionally in seven samples. Second, all samples are from petrologically well-characterized suites (see references in Table 1). Mineral assemblages, mineral compositions, and modes have been determined for all samples, and bulk $\delta^{13}C$ and $\delta^{18}O$ of carbonate have been measured for most at the mm scale by conventional phosphoric acid techniques. Sample numbers in Table 1 correspond to those in the relevant publications. Third, because the ion microprobe was operated with a ~5 to ~15 μm diameter beam, samples with grains ~50 μm in diameter or larger are essential to assess intracrystalline isotope zoning. Fourth, all samples contain abundant silicate minerals that were produced by decarbonation reactions during metamorphism. Because of the fractionation of carbon and oxygen isotopes among carbonates, silicates, and CO_2, evidence for decarbonation reactions assures that the carbon and oxygen isotope composition of minerals in the samples changed during metamorphism (Valley, 1986). In most samples the expected change in $\delta^{13}C$ and $\delta^{18}O$ is verified by bulk values of calcite and dolomite measured by conventional methods that are significantly lower than in unaltered marine carbonate rocks (e.g., $\delta^{13}C < -1‰$ and $\delta^{18}O < 20‰$). The decarbonation reactions in all samples are inferred to have been driven by infiltration of rocks by chemically reactive fluid (see references in Table 1), and the infiltration is a second mechanism by which the $\delta^{13}C$ and $\delta^{18}O$ of the rocks may have changed during metamorphism. It was anticipated that changes in $\delta^{13}C$ and $\delta^{18}O$ caused by decarbonation and infiltration might be preserved by intracrystalline and/or intercrystalline heterogeneity in $\delta^{13}C$ and $\delta^{18}O$. Finally, almost all samples were chosen to be as free as possible of retrograde alteration, such as serpentine, chlorite, and secondary dolomite, to avoid confusing the isotopic effects of prograde metamorphism with the effects of retrograde metamorphism. The exceptions are two samples of brucite marble in which brucite is secondary after periclase. Periclase marble, to our knowledge, is unknown because periclase is completely altered, or nearly so, to brucite by retrograde fluid flow during contact metamorphism (e.g., Ferry and Rumble, 1997).

The 19 samples in Table 1 are divided into five groups based on their petrologic context. The broadest subdivision is between regional (3 samples) and contact (16 samples) metamorphic rocks. Contact metamorphic rocks were favored for three reasons. First, isotopic heterogeneities have less opportunity to be erased by diffusion or recrystallization during contact metamorphism because of its shorter duration. Second, the interpretation of isotopic heterogeneity in contact metamorphic rocks is simpler because heat and fluid transport are better understood in contact aureoles than in regional metamorphic terrains, and in many cases unmetamorphosed protoliths can be identified and sampled. Third, invisible graphite inclusions lying just below the surface in the solid rock disks used as samples would fatally compromise a $\delta^{13}C$ analysis by ion microprobe. Graphite-free carbonate rocks are more common in contact aureoles than in regional metamorphic terrains likely because contact aureoles are often infiltrated during metamorphism by oxidizing fluids. Contact metamorphic rocks were favored to avoid graphite-bearing samples.

All three regional metamorphic rocks are from the Barrovian terrain in eastern Vermont, USA. Pressure (P) recorded by mineral equilibria was 7–8 kbars. Samples were collected in the biotite and garnet zones where mineral equilibria record temperature (T) ~475–500 °C. Because carbonate minerals in marls and limestones from the area contain high concentrations of graphite inclusions, the selected samples are metamorphic equivalents of volcanic and volcaniclastic rock and calcareous shale (all now graphite-free schists). Fig. 2a is a backscattered electron (BSE) image of sample 21-26E, the calc-schist. Metamorphic decarbonation reactions produced combinations of biotite, actinolite, and garnet in the three samples.

Selected contact metamorphic rocks are from the Mt. Morrison, Ritter Range, and Twin Lakes pendants in the Sierra Nevada, California, USA; from the Beinn an Dubhaich aureole in Scotland; and from the Monzoni and Predazzo aureoles in Italy. Pressure during metamorphism was 0.5–1.8 kbars, and T recorded by mineral equilibria is in the range 560–710 °C. The contact metamorphic rocks are further divided into four groups.

Table 1
Summary of geologic and petrologic information about samples investigated.

Group[a]	Sample	Location	Age (Ma)	Lithology/Petrology	T (°C)	P (kbars)	Mineralogy[b]	$\delta^{18}O^{c}$ (‰)	$\delta^{13}C^{c}$ (‰)	Ref.[d]
Reg Met	21-26E	Gile Mountain Fm., VT, USA	~355	Calc-schist, Grt zone	500	~7–8	Cal–Qtz–Pl–Ms–Bt–Grt	NA	NA	1, 2
Reg Met	C4A	Ammonoosuc Volcs., VT, USA	~355	Metavolcaniclastic rock, Bt zone	475	~7–8	Cal–Qtz–Pl–Bt–Chl	NA	NA	1, 2, 3
Reg Met	H4E	Ammonoosuc Volcs., VT, USA	~355	Metavolcanic rock, Bt zone	475	~7–8	Cal–Pl–Ep–Act–Chl	NA	NA	1, 2, 3
Cal-Sil H/M	KP1B	Twin Lakes pendant, CA, USA	80–100	Calc-silicate marble	595[e]	~1.8[e]	Di–Dol–Fo–Cal	21.5	−0.6	4
Cal-Sil H/M	KP1E	Twin Lakes pendant, CA, USA	80–100	Calc-silicate hornfels	595[e]	~1.8[e]	Cal–Wo–Di–Qtz	NA	NA	4
Cal-Sil H/M	KP2H	Twin Lakes pendant, CA, USA	80–100	Calc-silicate hornfels	595[e]	~1.8[e]	Cal–Wo–Di–Qtz	NA	NA	4
Cal-Sil H/M	KP3E	Twin Lakes pendant, CA, USA	80–100	Calc-silicate hornfels	595[e]	~1.8[e]	Cal–Wo–Di–Qtz–Grs–An	19.4	−1.3	4
Cal-Sil H/M	R3B	Ritter Range pendant, CA, USA	~91	Calc-silicate marble	595	1.5	Cal–Wo–Kfs–Grs–Pl–Di–Qtz	18.2[f]	−5.2	5
Cal-Sil H/M	R3L	Ritter Range pendant, CA, USA	~91	Calc-silicate marble	595	1.5	Cal–Di–Kfs–Pl–Qtz	18.3[f]	−4.7	5
Brc Marble	B4Q	Beinn an Dubhaich aureole, Scotland	54	Marble	700	0.5	Cal–Brc	10.2[f]	−2.9	6
Brc Marble	EM10C	Monzoni aureole, Italy	214–245	Marble	710	0.5	Cal–Brc	21.7[f]	+1.2	7
Rxn Front	B43A	Beinn an Dubhaich aureole, Scotland	54	Vein in marble	655[g]	0.5	Fo–Cal vein in Dol marble	See	Fig. 3	6
Rxn Front	CL29F	Mt. Morrison pendant, CA, USA	~89	Metasandstone exactly at Wo isograd	560	1.5	Qtz–Cal–Kfs–Di–Wo	13.4[f]	−2.7	8, 9
Rxn Front	CL30A	Mt. Morrison pendant, CA, USA	~89	Metasandstone exactly at Wo isograd	560	1.5	Qtz–Cal–Kfs–Di–Wo	13.3[f]	−1.7	8, 9
Rxn Front	KP1L	Twin Lakes pendant, CA, USA	80–100	Vein in marble	595[e]	~1.8[e]	Fo–Cal vein in Dol marble	11.1	−3.9	4
Perv Rxn	B1W	Beinn an Dubhaich aureole, Scotland	54	Marble	690	0.5	Dol–Fo–Cal	NA	NA	6
Perv Rxn	B3R	Beinn an Dubhaich aureole, Scotland	54	Marble	710	0.5	Dol–Fo–Cal	21.5[f]	−1.3	6
Perv Rxn	B4L	Beinn an Dubhaich aureole, Scotland	54	Marble	680	0.5	Dol–Fo–Cal	NA	NA	6
Perv Rxn	P2A	Predazzo aureole, Italy	232–238	Marble	710	0.5	Dol–Brc–Cal	24.9[f]	+1.7	7

[a] *Abbreviations for sample groups:* Reg Met, Barrovian regional metamorphic rocks; Cal-Sil H/M, calc-silicate hornfels and marble; Brc marble, brucite marble; Rxn Front, sample that contains a mineral reaction front; Perv Rxn, sample that contains a pervasive distribution of reactant and products of a mineral reaction.

[b] *Mineral abbreviations:* Act, actinolite; Brc, brucite; Bt, biotite; Cal, calcite; Chl, chlorite; Di, diopside; Dol, dolomite; Ep, epidote; Fo, forsterite; Grs, grossular; Grt, garnet; Kfs, K-feldspar; Ms, muscovite; Pl, plagioclase; Qtz, quartz; Wo, wollastonite.

[c] Analysis of bulk carbonate extracted by dental drill using conventional phosphoric acid methods on mg-sized samples from mm-sized domains as described in the relevant reference. Values of $\delta^{18}O$ relative to VSMOW; values of $\delta^{13}C$ relative to VPDB. NA, not analyzed. Value for sample KP1L refers to Cal in the Fo–Cal vein.

[d] *References:* (1) Ferry (1994), (2) Wing et al. (2003), (3) Ferry (1988), (4) Davis and Ferry (1993), (5) Ferry et al. (1998), (6) Ferry and Rumble (1997), (7) Ferry et al. (2002), (8) Ferry et al. (2001), and (9) Lackey and Valley (2004).

[e] New values of T estimated from the maximum Mg content of calcite inclusions in forsterite in sample KP1B. New value of P is the midpoint of the range of pressures consistent with equilibrium among diopside, dolomite, forsterite, calcite and CO_2–H_2O fluid in sample KP1B at 595 °C.

[f] Reported values reduced from published published values by 0.3‰ following recalibration of the laboratory's working calcite standard against NBS-19 in 2003.

[g] Estimated from the maximum Mg content of calcite inclusions in forsterite in sample B43A.

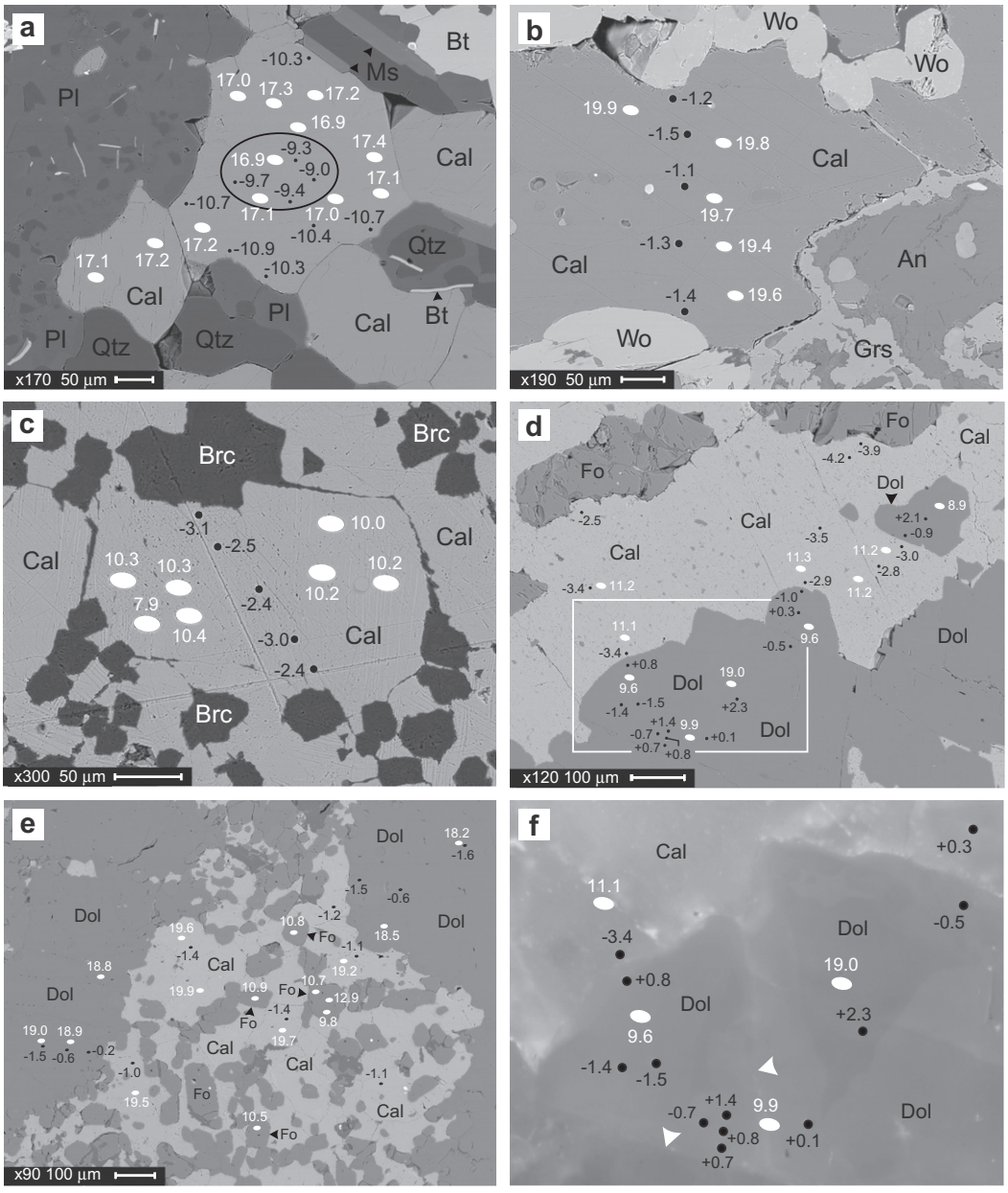

Fig. 2. BSE (a–e) and CL (f) images of representative analyzed samples. White ovals are locations of oxygen isotope analyses with size and shape the same as the analysis pits; white numbers are $\delta^{18}O$ (‰, VSMOW). Black circles are locations of carbon isotope analyses with size and shape the same as the analysis pits; black numbers are $\delta^{13}C$ (‰, VPDB). Magnification is an instrument setting, not magnification of the printed image. Cal, calcite; Qtz, quartz; Pl, plagioclase; Bt, biotite; Ms, muscovite; Wo, wollastonite; An, anorthite; Grs, grossularite; Brc, brucite; Dol, dolomite; Fo, forsterite. See Table 1 for details about each sample. (a) Regionally metamorphosed calcareous schist, sample 21-26E, grain #4. Black oval surrounds four analysis locations in the core of the grain where $\delta^{13}C$ is higher than at the other six locations closer to the margin of the grain. In contrast, the entire grain is uniform in $\delta^{18}O$ within error of measurement. (b) Contact metamorphosed calc-silicate hornfels, sample KP3E. Both $\delta^{13}C$ and $\delta^{18}O$ are uniform in the calcite grain within error of measurement. (c) Contact metamorphosed brucite marble, sample B4Q. Large scratches developed after ion microprobe analysis during removal of the Au coat. Values of $\delta^{13}C$ but not $\delta^{18}O$ are uniform within the analyzed calcite grain. Zoning in $\delta^{18}O$ is patchy rather than concentric. (d) Reaction front at the margin of a forsterite–calcite vein in host dolomite marble, sample KP1L. Calcite is uniform in $\delta^{18}O$ within error of measurement. Calcite is inhomogeneous in $\delta^{13}C$, and dolomite is inhomogeneous in both $\delta^{13}C$ and $\delta^{18}O$. Variations in $\delta^{13}C$ and $\delta^{18}O$ in dolomite are up to 3.7‰ and up to 9.4‰, respectively. White rectangle outlines the region illustrated in Fig. 2f. (e) Coexisting reactant (dolomite) and products (forsterite + calcite) of Reaction (3), sample B1W. Within the field of view, values of $\delta^{13}C$ in calcite and dolomite are uniform within error of measurement with compositions consistent with isotope exchange equilibrium. In contrast, some grains of calcite and dolomite are not in oxygen isotope exchange equilibrium. The $\delta^{18}O$ of forsterite exhibits significant intracrystalline and intercrystalline variations, and forsterite compositions are inconsistent with isotope exchange equilibrium with calcite and dolomite. (f) CL image of region within white rectangle in (d) taken with the luminoscope at the Smithsonian Institution. Variability in $\delta^{13}C$ and $\delta^{18}O$ in dolomite correlates with variability in CL brightness. The variability in CL brightness, in turn, is in part associated with faint linear features that are healed fractures (marked by white arrowheads).

One group, calc-silicate hornfels and marble, is composed primarily of calcite and the calc-silicate minerals diopside and wollastonite. Hornfelses contain more silicates and less calcite than marbles. Sample KP3E from the Twin Lakes pendant is a representative hornfels (Fig. 2b). One marble sample (R3L) contains calcite and quartz because it escaped infiltration by low X_{CO_2} fluid that produced wollastonite in other rocks from the Ritter Range pendant like sample R3B. Another (KP1B) contains dolomite and forsterite. Less abundant minerals may include combinations of plagioclase, K-feldspar, and grossularite. The metamorphic reaction(s) that produced diopside, wollastonite, and other calc-silicate minerals in the hornfelses and marbles went to completion or nearly so, and the initially least abundant reactant mineral is rare or absent.

A second group of contact metamorphic rock is brucite marble that is essentially just calcite and brucite. Sample B4Q from the Beinn an Dubhaich aureole is representative (Fig. 2c). The protolith was dolomite that lost half its CO_2 by the reaction,

$$\text{dolomite} = \text{periclase} + \text{calcite} + CO_2 \quad (1)$$

Reaction (1) went to completion, and periclase was later hydrated to brucite. The two samples selected are unusual for containing no secondary dolomite.

Samples in a third group capture a reaction front that separates reactant and product minerals across a sharp interface. The arrested reaction in the two samples from the Mt. Morrison pendant is

$$\text{calcite} + \text{quartz} = \text{wollastonite} + CO_2. \quad (2)$$

The samples additionally contain diopside and K-feldspar. Based on field relations, sample CL29F captures reaction at the side of a fluid flow channel, and sample CL30A captures reaction at right angles to the flow direction. Sample KP1L from the Twin Lakes pendant contains a forsterite–calcite vein that cuts nearly pure dolomite marble. The contact between vein and marble (Figs. 2d and f) represents the side of a fluid flow channel where the arrested reaction is

$$\text{dolomite} + SiO_2(aq) = \text{forsterite} + 2\text{calcite} + 2CO_2 \quad (3)$$

Dissolved SiO_2 was transported to the reaction site by the vein-forming fluid. Sample B43A from the Beinn an Dubhaich aureole is also of a forsterite–calcite vein in dolomite marble, but the vein is so thick that only one contact between vein and dolomite is captured. Material for $\delta^{13}C$ and $\delta^{18}O$ analyses was collected with a dental drill along traverses across both veins. Results (Fig. 3) suggest that small-scale heterogeneities in both $\delta^{13}C$ and $\delta^{18}O$ were to be expected at the two reaction fronts.

The fourth group contains coexisting reactants and products of a contact metamorphic decarbonation reaction that are more evenly distributed than in the samples that contain a sharp reaction front. The three samples from the Beinn an Dubhaich aureole represent an arrested state of Reaction (3); sample B1W is representative (Fig. 2e). The sample from the Predazzo aureole represents an arrested state of Reaction (1).

4. SAMPLE PREPARATION

Samples were cut into 2.54-cm diameter circular disks. Rock disks were used instead of thin sections to minimize possible contamination from epoxy during $\delta^{13}C$ analyses. Two grains each of one or two carbonate standards were mounted with one or two drops of epoxy in a 1-mm

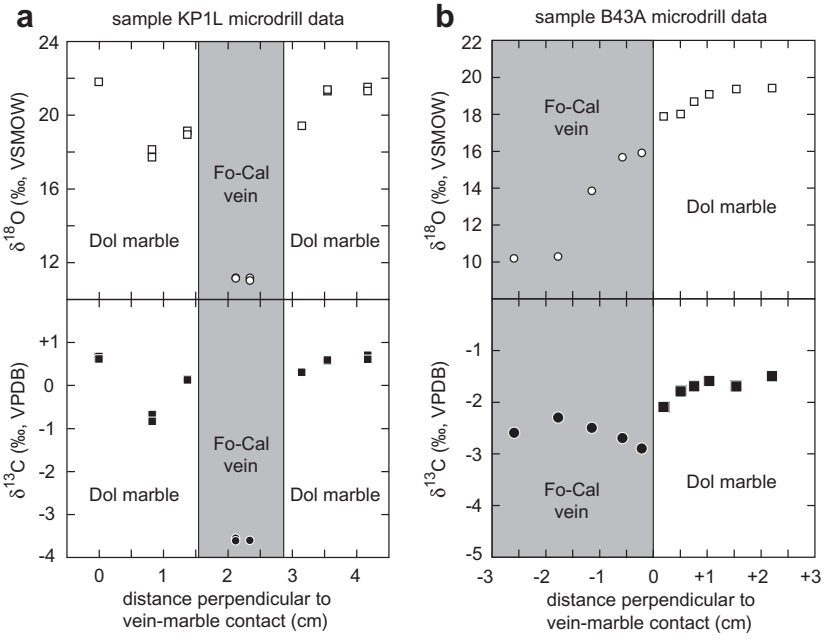

Fig. 3. Profiles in $\delta^{18}O$ and $\delta^{13}C$ across the contact between two forsterite–calcite veins and their host dolomite marble. Uncertainties (±2SD) are approximately the size of the symbols. Steep gradients in isotope composition at the cm-scale correlate with variability in $\delta^{13}C$ and $\delta^{18}O$ at the sub-mm scale. (a) Sample KP1L. Data collected by conventional analysis as part of this study. (b) Sample B43A. Data are from Wing et al. (2000).

diameter hole drilled ~300 μm deep in the center of the sample. The side of the disk with the standard(s) was then polished with special care to minimize surface relief, as recommended by Kita et al. (2009), and the opposite side trimmed to reduce the disk to 5 mm thickness. A separate standard mount was made for $\delta^{18}O$ analysis with grains of calcite, dolomite, quartz, and olivine standards imbedded in epoxy, polished, and trimmed to 5 mm thickness.

Cathodoluminescence (CL) and BSE images were obtained of polished uncoated samples and the standard mount with the Hitachi S3400N variable pressure scanning electron microscope in the Department of Geoscience at the University of Wisconsin, Madison. Several areas of interest for analysis were located in each rock sample, almost all within 5 mm of the center of the disk. In some cases, the areas of interest were reexamined in CL with the ELM-3 Luminoscope and an Olympus Magnafire Imaging System in the laboratory of Sorena S. Sorensen at the National Museum of Natural History, Smithsonian Institution. Finally, all samples were photographed with a reflected light microscope, cleaned by multiple rinsings and sonication with ethanol and distilled water, and coated with a ~30 nm layer of Au.

5. ANALYTICAL METHODS

Carbon isotope analyses of calcite and dolomite and oxygen isotope analyses of calcite, dolomite, quartz, and forsterite were obtained with the CAMECA ims-1280 ion microprobe in the Department of Geoscience at the University of Wisconsin, Madison, using operating and analytical conditions described in detail by Kita et al. (2009). The Cs^+ primary beam (20 keV total accelerating voltage) was focused to a diameter of ~5–15 μm on the sample surface (depending on the session) and the secondary C^- and O^- ions were accelerated by −10 kV using an electron gun for charge compensation. The primary ion intensities were ~2 nA for oxygen isotope analyses and 0.3–0.6 nA for carbon isotope analyses. The secondary optics were similar to those in Kita et al. (2009) that achieve high secondary ion transmission. Detailed alignment included transfer lens magnification of 200, contrast aperture 400 μm diameter, field aperture 4000 × 4000 μm square, entrance slit 122 μm width, and energy slit 40 eV width. The exit slit was set at 500 μm width for oxygen isotope analyses and 300 μm width for carbon isotope analyses, corresponding to a mass resolving power of ~2500 and ~4000, respectively. These mass resolving powers were sufficient to separate hydride interferences on ^{18}O and ^{13}C.

For oxygen isotope analysis, two Faraday cup (FC) detectors, used to simultaneously measure ^{16}O and ^{18}O, were equipped with different amplifiers (10^{10} and 10^{11} Ω resistors, respectively). The measured intensity of ^{16}O was ~2×10^9 cps (~10^9 cps/nA). The baseline of the FC amplifiers was calibrated once per day, and drift during the day was insignificant compared to the noise levels of the detectors (⩽1000 cps for the 10^{11} Ω FC). For carbon isotope analysis, one FC equipped with a 10^{11} Ω resistor amplifier and one electron multiplier detector were used to simultaneously measure ^{12}C and ^{13}C. The measured intensity of ^{12}C was (0.4–0.6) × 10^7 cps (~10^7 cps/nA). The baseline of the amplifier was calibrated once per day. The gain of the electron multiplier was monitored before the third analysis of each group of four standard calcite analyses, and the applied high voltage was adjusted to compensate drift of the gain of the electron multiplier, if necessary. Reproducibility of $\delta^{13}C$ of the bracketing standard analyses includes the drift of the gain of the electron multiplier. At each analysis position, any small misalignment of the secondary optics was automatically tuned by scanning deflectors before the isotope measurement started.

Measurements of $\delta^{13}C$ and $\delta^{18}O$ were made on different but nearby points (e.g., Fig. 2). Total time per analysis was ~3–5 min, including time for locating the analytical position, pre-sputtering (10 s for oxygen, 20 s for carbon), automatic tuning of the secondary ions, and analysis (80 s for oxygen; 160 s for carbon).

Data were corrected for the instrumental bias using either UWC1 calcite standard ($\delta^{18}O = 23.36‰$ VSMOW, $\delta^{13}C = -2.03‰$ VPDB) or UWC3 calcite standard ($\delta^{18}O = 12.49‰$ VSMOW, $\delta^{13}C = -0.91‰$ VPDB, Kozdon et al., 2009). For carbon isotope analysis of dolomite, the difference in bias between calcite and dolomite (Cal–Dol) was calibrated by analysis of the calcite standard and UW6220 dolomite standard ($\delta^{18}O = 22.72‰$ VSMOW, $\delta^{13}C = +0.79‰$ VPDB) measured in the same mount during the same analytical session. The difference in bias between calcite and dolomite during carbon isotope analysis was 2.2‰ for UWC1 (one analytical session) and 1.3–3.0‰ for UWC3 (varying over three sessions spread out over 15 months). Standards used during oxygen isotope analysis of calcite, dolomite, quartz, and forsterite were UWC1 calcite, UWC3 calcite, UW6220 dolomite, UWQ1 quartz ($\delta^{18}O = 12.33‰$ VSMOW, Kelly et al., 2007), and San Carlos olivine ($\delta^{18}O = 5.32‰$ VSMOW, Kita et al., 2010). For oxygen isotope analysis, the difference in instrumental bias between calcite and dolomite, calcite and quartz, and calcite and forsterite was 5.1‰, 1.2‰, and −8.5‰, respectively. Standards were measured four times every 10–12 unknown analyses. The bias correction was based on the average of four standard calcite analyses made before and after the group of unknowns (eight total analyses of the standard). In one session of carbon isotope analysis, a linear drift correction was applied to all measured data because the measured composition of the calcite standard changed systematically over the duration of the session. Drift was not detected in any of the other sessions. The average spot-to-spot reproducibility, or "analytical uncertainty" in the terminology of Kita et al. (2009), of analyses of unknowns was considered ±2SD (SD, standard deviation) of the eight bracketing calcite standard analyses. For all $\delta^{18}O$ measurements, the average 2SD was 0.37‰ (range, 0.14–0.73‰), and for all $\delta^{13}C$ measurements, the average 2SD was ±0.71‰ (range, 0.33–1.13‰). Carbon and oxygen isotope ratios were normalized to VPDB and VSMOW and reported as $\delta^{13}C$ and $\delta^{18}O$.

Measured values of $\delta^{13}C$ and $\delta^{18}O$ of calcite and dolomite were corrected for Mg content using the measured difference in bias between calcite and dolomite standards and assuming a linear dependence of bias on the mole fractions

of $MgCO_3$ and $CaMg(CO_3)_2$ in calcite and dolomite, respectively (Valley and Kita, 2009). The maximum correction to $\delta^{18}O$ for the Mg content of calcite and dolomite was +0.35‰ and −0.16‰, respectively. The maximum correction to $\delta^{13}C$ of calcite and dolomite was +0.21‰ and −0.08‰, respectively. The minimum corrections to $\delta^{18}O$ for calcite and dolomite were 0.00‰ and −0.07‰, respectively, and 0.00 and −0.02‰ to $\delta^{13}C$, respectively. No correction of bias was necessary for the difference in composition between the San Carlos olivine standard and analyzed Fo in the samples investigated (Kita et al., 2010).

Every analysis pit for both $\delta^{13}C$ and $\delta^{18}O$ was examined by BSE imaging to evaluate whether any were contaminated by inclusions of other minerals or were in a potentially problematic textural site such as along a fracture or grain boundary. Only four such analysis pits were identified, and they all lie along fractures. Interpretation of the analyses at the four spots accordingly is uncertain as is later discussed in Section 6.2.

6. RESULTS

All measurements by ion microprobe of $\delta^{13}C$ and $\delta^{18}O$ of the standards and unknowns, selected instrument settings and readings for each analysis, details of the corrections for instrumental bias, and measured compositions of calcite and dolomite in all analyzed samples are compiled in the Electronic annex.

6.1. Carbon isotope analyses

Table 2 summarizes all 398 measurements of $\delta^{13}C$ of calcite and dolomite in the 19 analyzed samples. Figs. 4–7 illustrate all analyses grouped by petrologic context: regional metamorphic rock (Fig. 4), calc-silicate hornfels and marble and brucite marble (Fig. 5), samples that contain a pervasive distribution of reactants and products (Fig. 6), and samples that contain a reaction front (Fig. 7). The format of all diagrams is the same as described in the figure captions. To facilitate comparison, all but two diagrams span a range of 5‰ in $\delta^{13}C$; for two samples (KP1L, CL30A, Fig. 7) a range of 9‰ was needed to include a wider variation in measured values. Fig. 8 summarizes all $\delta^{13}C$ measurements of calcite, and Fig. 9 summarizes all $\delta^{13}C$ measurements of coexisting calcite and dolomite.

In most samples, 2–4 grains were selected and 5–17 analyses were obtained along traverses across each grain (Fig. 2 illustrates examples). Together, the data allow for evaluation both of the variation of $\delta^{13}C$ within grains and between grains in the same sample. When all or almost all analyses in a sample are the same at a 95% confidence level, analyses from the different grains are not distinguished in Figs. 4–7. When grains are zoned in $\delta^{13}C$ and/or there is significant grain-to-grain variation within the sample, results for the different analyzed grains are distinguished. Most analyses illustrated in Fig. 6 are from different calcite and dolomite grains because samples that contain a pervasive distribution of mineral reactants and products are finer grained than the others.

Because the principal goal of the study was to search for small-scale isotopic heterogeneity in the samples, meanings of "homogeneous" and "inhomogeneous" or "heterogeneous" were defined quantitatively. An individual grain or entire sample is defined as "homogeneous" if all analyses of it are consistent with the same value of $\delta^{13}C$ (or $\delta^{18}O$) at a 95% confidence level based on the mean square weighted deviate, MSWD (Mahon, 1996). Values of MSWD for a population of analyses were computed from the measured $\delta^{13}C$ (or $\delta^{18}O$) values and their 1SD analytical uncertainties (1SD of the eight bracketing analyses of the calcite standard). A grain or entire sample is defined as "inhomogeneous" or "heterogeneous" if two or more measured values of $\delta^{13}C$ (or $\delta^{18}O$) within the grain or sample differ by >6SD. Because values of SD are always based on eight measurements of the standard, the definition of "inhomogeneous" and "heterogeneous" corresponds to a ~97% confidence interval according to Student's *t*-test (Mahon, 1996). An individual analysis that is inconsistent with homogeneity according to the criterion defined by the MSWD but that does not differ from any other analysis in the grain or sample by >6SD is termed an "inconclusive outlier." A separate category of "inconclusive outlier" was established to avoid the situation in which the conclusion whether a single grain or population of grains is homogeneous or heterogeneous is based on a very small difference in $\delta^{13}C$ (or $\delta^{18}O$) between two analyses (a few hundredths per mil, for example).

Among the three analyzed samples of regional metamorphic rock (Figs. 4 and 8), one (H4E) contains calcite that is homogeneous in $\delta^{13}C$ (no measurable intracrystalline or intercrystalline inhomogeneity), one (C4A) contains calcite that is homogenous with the exception of a single inconclusive outlier, and one (21-26E) contains calcite that displays both intracrystalline and intercrystalline inhomogeneity in $\delta^{13}C$. Maximum and minimum measured values of $\delta^{13}C$ in grain #4, sample 21-26E, differ by >6SD. The largest values consistently occur in the core of the grain, and the smallest values near the margin (Fig. 2a), apparently defining concentric $\delta^{13}C$ zoning. The spatial variation in $\delta^{13}C$ within grain #4 is not correlated with any concentric variation in CL brightness. A MSWD value of 5.89 calculated from the 10 analyses of grains #2 and #5 is too large to be consistent with a population of uniform $\delta^{13}C$ values at a 95% confidence level. The maximum value of $\delta^{13}C$ measured in grain #2 differs by >6SD from the minimum value in grain #5, indicating that the difference in $\delta^{13}C$ between the two grains is significant according to the criterion adopted in this study.

Among the six samples of calc-silicate hornfels and marble (Figs. 5 and 8), three contain calcite that is homogenous in $\delta^{13}C$ (KP1E, KP2H, R3L), and three contain homogeneous calcite except for one (KP3E, R3B) or two (KP1B) inconclusive outliers. Data from samples KP1B and KP2H demonstrate that $\delta^{13}C$ of calcite inclusions in calc-silicate minerals (wollastonite or diopside) is the same as $\delta^{13}C$ of the matrix calcite. One of the brucite marbles (Figs. 2c and 8) contains calcite that is homogenous in $\delta^{13}C$ (B4Q), and the other contains homogeneous calcite except for a single inconclusive outlier (EM10C). All four samples

Table 2
Summary of carbon and oxygen isotope compositions measured by ion microprobe analysis of 5–15 μm spots at WiscSIMS.

Group[a]	Reg Met	Reg Met	Reg Met	Reg Met	Cal-Sil H/M	Cal-Sil H/M	Cal-Sil H/M	Cal-Sil H/M
Sample	21-26E	21-26E	C4A	H4E	KP1B	KP1E	KP2H	KP3E
Isotope	C	O	C	C	C	C	C	C
Mineral[a]	Cal	Cal	Cal	Cal	Cal	Cal	Cal	Cal
No. analyses	20	12	15	15	17	15	17	20
Range δ (‰)	−10.9 to −7.9	16.9–17.4	−7.5 to −5.9	−2.2 to −0.6	−1.1 to +1.1	−0.7 to +0.4	−1.0 to +0.6	−1.9 to −0.6
2SD δ (‰)	0.61	0.35	0.70	0.77–1.13	0.68–0.93	0.65	0.68–1.02	0.54
MSWD[b]	Inhomog	0.86	1.61	1.10	1.79	1.25	1.08	1.51
$n_{omitted}/n_{total}$[c]	Inhomog	0/12	1/15	0/15	2/17	0/15	0/17	1/20
Wt. mean[d]	Inhomog	17.12 ± 0.11	−6.86 ± 0.20	−1.36 ± 0.27	+0.03 ± 0.21	−0.26 ± 0.18	−0.12 ± 0.20	−1.39 ± 0.13
Group[a]	Cal-Sil H/M	Cal-Sil H/M	Cal-Sil H/M	Cal-Sil H/M	Brc Marble	Brc Marble	Brc Marble	Rxn Front
Sample	KP3E	R3B	R3L	R3L	B4Q	B4Q	EM10C	B43A
Isotope	O	C	C	O	C	O	C	C
Mineral[a]	Cal	Cal	Cal	Cal	Cal	Cal	Cal	Cal
No. analyses	10	15	16	11	15	12	15	22
Range δ (‰)	19.3–19.9	−5.5 to −4.5	−5.5 to −3.7	17.9–18.7	−3.3 to −2.4	7.9–10.4	+1.9 to +3.5	−2.1 to −0.2
2SD δ (‰)	0.44	0.33	0.82–0.91	0.24	0.56	0.24	0.63–0.64	0.63–1.04
MSWD[b]	0.69	1.82	1.29	1.88	1.20	2.07	1.59	1.14
$n_{omitted}/n_{total}$[c]	0/10	1/15	0/16	1/11	0/15	2/12	1/15	1/22
Wt. mean[d]	19.57 ± 0.16	−4.87 ± 0.10	−4.81 ± 0.23	18.37±0.09	−2.74 ± 0.16	10.12 ± 0.09	+2.49 ± 0.19	−1.36 ± 0.17
Group[a]	Rxn Front	Rxn Front	Rxn Front	Rxn Front	Rxn Front	Rxn Front	Rxn Front	Rxn Front
Sample	B43A	B43A	B43A	B43A	CL29F	CL29F	CL29F	CL30A
Isotope	O	C	O	O	C	O	O	C
Mineral[a]	Cal	Dol	Dol	Fo	Cal	Cal	Qtz	Cal
No. analyses	16	18	15	9	10	5	5	26
Range δ (‰)	3.3–18.2	−2.3 to −0.7	16.9–18.1	12.1–15.0	−4.1 to −1.8	13.2–13.8	15.6–16.0	−4.1 to +1.5
2SD δ (‰)	0.40–0.72	0.63–1.04	0.53–0.73	0.45–0.54	0.62	0.36	0.39	0.41–0.94
MSWD[b]	Inhomog	1.34	1.27	Inhomog	Inhomog	1.83	0.55	Inhomog
$n_{omitted}/n_{total}$[c]	Inhomog	0/18	0/15	Inhomog	Inhomog	0/5	0/5	Inhomog
Wt. mean[d]	Inhomog	−1.41 ± 0.10	17.37 ± 0.16	Inhomog	Inhomog	13.45 ± 0.26	15.84 ± 0.28	Inhomog
Group[a]	Rxn Front	Rxn Front	Rxn Front	Rxn Front	Rxn Front	Rxn Front	Rxn Front	Perv Rxn
Sample	CL30A	CL30A	KP1L	KP1L	KP1L	KP1L	KP1L	B1W
Isotope	O	O	C	O	C	O	O	C
Mineral[a]	Cal	Qtz	Cal	Cal	Dol	Dol	Fo	Cal
No. analyses	15	15	20	15	28	15	10	6
Range δ (‰)	12.6–13.4	14.8–16.3	−4.5 to −2.5	10.6–11.3	−1.5 to +2.4	8.9–19.0	6.4–7.2	−1.5 to −1.0
2SD δ (‰)	0.27–0.39	0.31–0.40	0.43–0.93	0.36–0.51	0.43–0.93	0.36–0.40	0.37–0.55	0.81
MSWD[b]	1.64	Inhomog	Inhomog	1.22	Inhomog	Inhomog	0.89	0.20
$n_{omitted}/n_{total}$[c]	1/15	Inhomog	Inhomog	0/15	Inhomog	Inhomog	0/10	0/6
Wt. mean[d]	12.90 ± 0.09	Inhomog	Inhomog	11.01 ± 0.11	Inhomog	Inhomog	6.77 ± 0.16	−1.19 ± 0.46
Group[a]	Perv Rxn	Perv Rxn	Perv Rxn	Perv Rxn	Perv Rxn	Perv Rxn	Perv Rxn	Perv Rxn
Sample	B1W	B1W	B1W	B1W	B3R	B3R	B4L	B4L
Isotope	O	C	O	O	C	C	C	O
Mineral[a]	Cal	Dol	Dol	Fo	Cal	Dol	Cal	Cal
No. analyses	10	6	10	11	15	15	15	7
Range δ (‰)	18.3–19.9	−1.6 to −0.2	18.2–19.0	9.8–17.2	−2.3 to −0.6	−2.7 to −0.8	−0.9 to +0.6	20.4–21.7
2SD δ (‰)	0.30	0.81	0.30–0.31	0.39	0.49–0.99	0.49–0.99	0.96–0.98	0.30–0.42
MSWD[b]	Inhomog	2.03	2.21	Inhomog	1.83	1.78	0.71	2.48
$n_{omitted}/n_{total}$[c]	Inhomog	0/6	2/10	Inhomog	0/15	1/15	0/15	1/7
Wt. mean[d]	Inhomog	−1.00 ± 0.46	18.70 ± 0.13	Inhomog	−1.52 ± 0.18	−1.41 ± 0.19	−0.15 ± 0.27	21.40 ± 0.19
Group[a]	Perv Rxn	Perv Rxn	Perv Rxn	Perv Rxn	Perv Rxn	Perv Rxn	Perv Rxn	
Sample	B4L	B4L	B4L	P2A	P2A	P2A	P2A	
Isotope	C	O	O	C	O	C	O	
Mineral[a]	Dol	Dol	Fo	Cal	Cal	Dol	Dol	
No. analyses	15	7	7	11	10	11	10	
Range δ (‰)	−1.1 to +0.5	20.8–21.5	18.5–19.3	+0.3 to +2.1	19.8–23.4	+0.7 to +2.3	22.9–23.7	
2SD δ (‰)	0.96–0.98	0.30–0.42	0.47	0.82–0.93	0.14–0.40	0.82–0.93	0.16–0.40	

(*continued on next page*)

Table 2 (*continued*)

Group[a]	Perv Rxn	Perv Rxn	Perv Rxn	Perv Rxn	Perv Rxn	Perv Rxn	Perv Rxn
Sample	B4L	B4L	B4L	P2A	P2A	P2A	P2A
MSWD[b]	0.77	2.12	1.25	1.20	Inhomog	1.42	1.94
$n_{omitted}/n_{total}$[c]	0/15	1/7	0/7	0/11	Inhomog	0/11	2/10
Wt. mean[d]	-0.45 ± 0.27	20.99 ± 0.25	18.79 ± 0.23	$+1.55 \pm 0.29$	Inhomog	$+1.79 \pm 0.29$	23.19 ± 0.10

[a] See footnotes of Table 1 for definition of abbreviations.
[b] MSWD, mean square weighted deviate (Mahon, 1996). Inhomog, inhomogeneous: two or more measured values differ by >6SD.
[c] $n_{omitted}/n_{total}$, number of analyses omitted from the calculation of the weighted mean divided by the total number of measurements.
[d] Wt. mean, weighted mean. Uncertainty is the 95% confidence interval calculated following Mahon (1996).

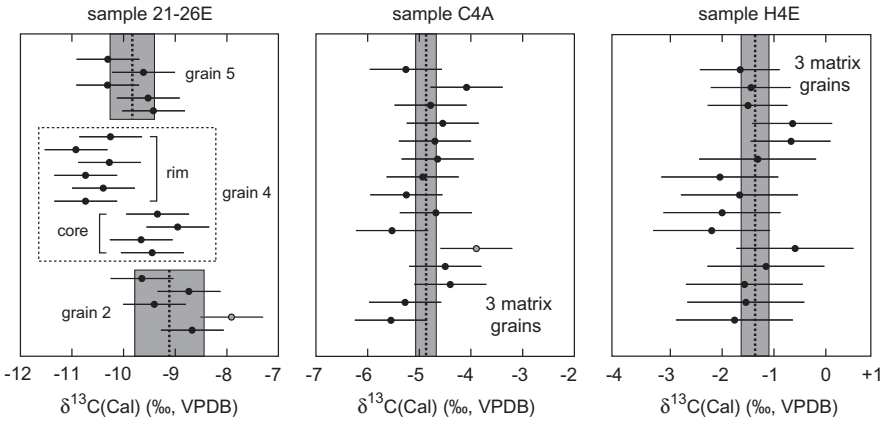

Fig. 4. All ion microprobe measurements of $\delta^{13}C$ of calcite (Cal) in the regional metamorphic rocks. Each symbol corresponds to an individual analysis, and the horizontal line through the symbol represents the ±2SD analytical uncertainty. A weighted mean (thick vertical dashed line) was computed for individual grains or groups of grains in a sample that are statistically consistent with a uniform value at a 95% level of confidence, as indicated by the mean square weighted deviate (MSWD, Mahon, 1996). Analyses used in the calculation of the weighted mean are shown as black symbols. The gray band is the 95% confidence interval of the weighted mean calculated following Mahon (1996). When all but one or two analyses for a sample or grain are consistent with a uniform value, the outliers are identified by a symbol with gray shading. A weighted mean was not computed for samples or grains that contain >2 outlying analyses. Data for different grains are distinguished where important; otherwise only the total number of different analyzed grains is noted. Fig. 2a is an image of grain #4, sample 21-26E.

with a pervasive distribution of reactants and products of Reactions (1) and (3), contain calcite that is homogeneous in $\delta^{13}C$ (Figs. 6 and 8). Three samples contain dolomite that is homogeneous as well, and the fourth (B3R) contains dolomite that is homogeneous in $\delta^{13}C$ except for a single inconclusive outlier (Figs. 6 and 9).

Among the contact metamorphic rocks investigated, significant inhomogeneity in $\delta^{13}C$ is limited to samples that contain a reaction front (Figs. 7–9). Only one of the four samples (B43A) contains carbonate that is homogeneous in $\delta^{13}C$ (dolomite) or homogeneous with the exception of a single inconclusive outlier (calcite). Individual calcite grains in sample CL29F (#4 and #5) and grains #1A, #1B, and #2A in sample CL30A are either homogeneous in $\delta^{13}C$ (#1A, #1B) or homogeneous with the exception of a single inconclusive outlier (#2A, #4, #5). Values of $\delta^{13}C$, however, differ between grains in both samples by >6SD. Sample CL29F exhibits intercrystalline inhomogeneity but no significant intracrystalline inhomogeneity. The maximum and minimum values of $\delta^{13}C$ for grain #8 in sample CL30A differ by >6SD. Sample CL30A exhibits both intercrystalline and intracrystalline heterogeneity. Because the outlying analysis spot in grain #8 is the same distance from the grain edge as two other analysis spots, the $\delta^{13}C$ zoning does not appear to be concentric.

Dolomite distal (>~1 cm) from the reaction front in sample KP1L is homogeneous in $\delta^{13}C$ except for a single inconclusive outlier. Two of three dolomite grains near the reaction front are homogeneous in $\delta^{13}C$ but have spot compositions different from spot compositions in the distal dolomite by >6SD. The third dolomite grain near the reaction front is very heterogeneous with intracrystalline differences in $\delta^{13}C$ of up to 3.8‰ (Fig. 2d). Seventeen $\delta^{13}C$ measurements of a single large calcite grain at the reaction front (in part, adjacent to the inhomogeneous dolomite grain) demonstrate that the grain is also inhomogeneous. A second analyzed calcite grain within the interior of the vein is homogeneous in $\delta^{13}C$. The largest $\delta^{13}C$ value measured in the calcite grain in the vein interior differs by >6SD from the smallest $\delta^{13}C$ value in the zoned calcite grain at the reaction front. Calcite and dolomite therefore display both significant intracrystalline and significant intercrystalline inhomogeneity in $\delta^{13}C$ in sample KP1L. The spatial distribution of $\delta^{13}C$ measurements in the zoned calcite and dolomite grains in sample KP1L defines irregular rather than concentric zoning (Fig. 2d). The variation in

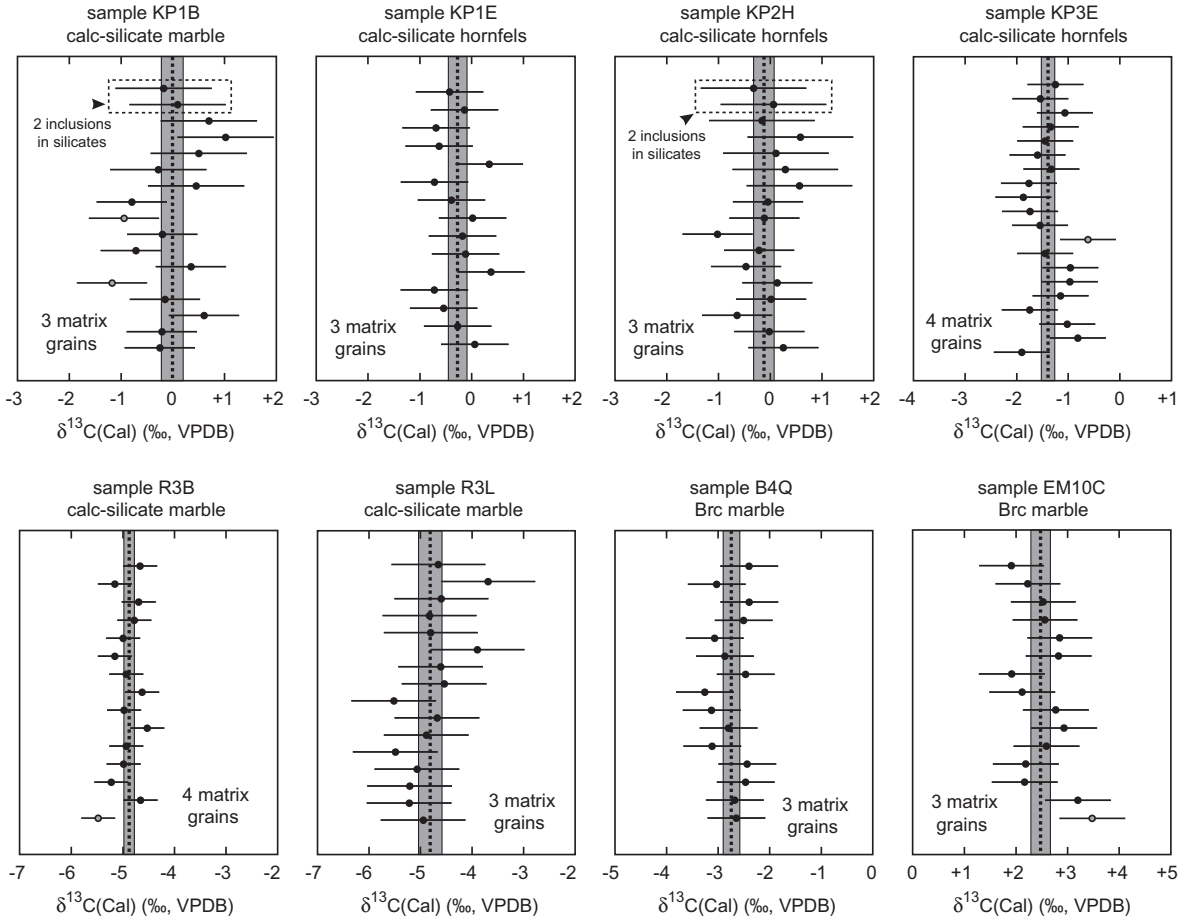

Fig. 5. All ion microprobe measurements of $\delta^{13}C$ of calcite in calc-silicate hornfels and marble and in brucite marble. Format is the same as in Fig. 4.

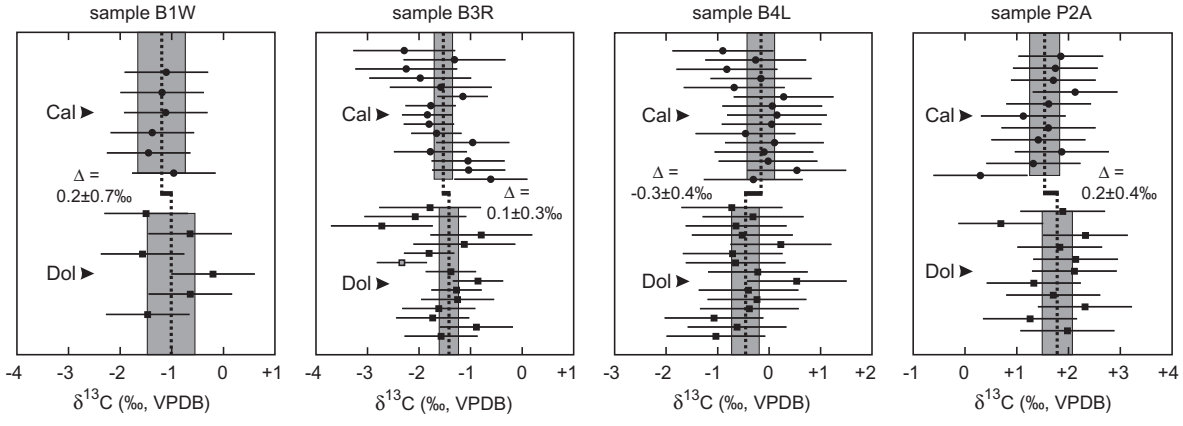

Fig. 6. All ion microprobe measurements of $\delta^{13}C$ of calcite and dolomite (Dol) in samples that contain a pervasive distribution of reactants and products of either Reaction (1) (P2A) or Reaction (3) (B1W, B3R, B4L). Format is the same as in Fig. 4. Thick horizontal bar and number value in each panel is $\Delta^{13}C$(Dol–Cal) based on the weighted mean $\delta^{13}C$ for calcite and dolomite in the sample. Because of the small grain size of the samples, most analyses are of different grains.

$\delta^{13}C$ within the dolomite grain in Fig. 2d is associated with faint irregular variation in CL brightness (Fig. 2f). The variation in CL brightness, in turn, appears to be partly related to healed fractures (identified by white arrowheads in Fig. 2f) that are also observed optically in thin section. In thin section, the healed fractures are loci of fluid inclusions

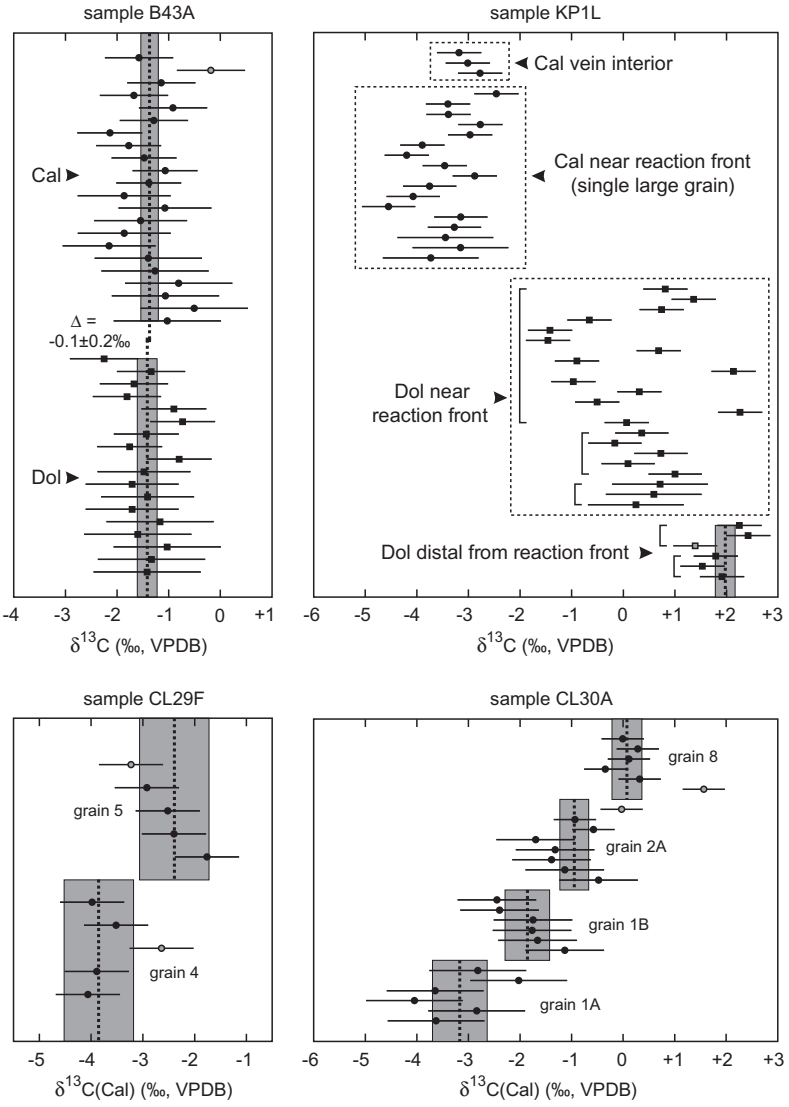

Fig. 7. All ion microprobe measurements of $\delta^{13}C$ of calcite and dolomite in samples that contain a reaction front involving either Reaction (2) (CL29F, CL30A) or Reaction (3) (B43A, KP1L). Format is the same as in Figs. 4 and 6. Analyses of the same dolomite grain in sample KP1L are grouped by a square bracket. Because of the small grain size of sample B43A, most analyses are of different grains. Sites of many of the Cal and Dol analyses in sample KP1L "near reaction front" are imaged in Fig. 2d.

and are typically confined to individual grains rather than traversing the entire sample.

6.2. Oxygen isotope analyses

Table 2 summarizes all 237 measurements of $\delta^{18}O$ of calcite, dolomite, quartz, and forsterite in 11 analyzed samples. All analyses of regional metamorphic rock (1 sample), calc-silicate hornfels and marble (2 samples), and brucite marble (1 sample) are illustrated in Fig. 10; all analyses of the four samples that contain a reaction front are illustrated in Fig. 11; and all analyses of three of the samples that contain a pervasive distribution of reactant and products are illustrated in Fig. 12. The format of Figs. 10–12 is the same as in Figs. 4–7.

Grain #4 in regional metamorphic sample 21-26E (Figs. 2a and 10) was analyzed to determine whether zoning in $\delta^{18}O$ is associated with zoning in $\delta^{13}C$. Ten analyses of $\delta^{18}O$ in grain #4 and two analyses of an adjacent grain demonstrate that there is no significant intracrystalline or intercrystalline inhomogeneity in $\delta^{18}O$ within the sample. The analyzed calc-silicate hornfels (KP3E, Fig. 2b) contains calcite that is homogenous in $\delta^{18}O$. Calc-silicate marble sample R3L contains homogeneous calcite except for a single outlier that differs from the largest measured value of $\delta^{18}O$ in the other analyzed grains in the sample by >6SD (Fig. 10). The $\delta^{18}O$ of the outlying analysis, however, does not differ by >6SD from other measured values in the same grain. The data therefore demonstrate that significant differences in $\delta^{18}O$ occur between grains in sample R3L, that some grains are homogeneous, and that other grains are neither homogeneous nor conclusively heterogeneous by the definitions used in this study. The analyzed sample of brucite marble (B4Q, Fig. 10) contains homogeneous calcite

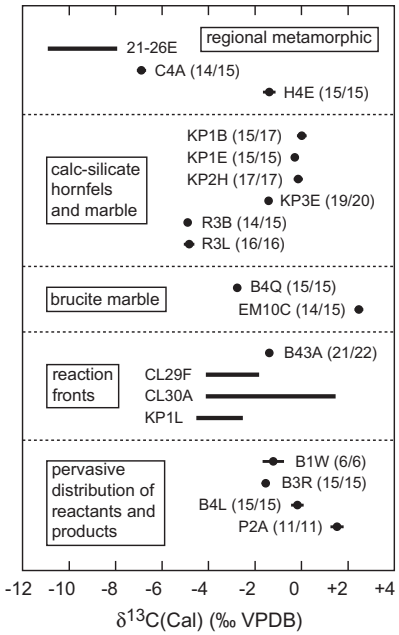

Fig. 8. Summary of all measurements of $\delta^{13}C$ of calcite grouped by petrologic context. Filled circles represent the weighted mean value for samples in which $\delta^{13}C$ is uniform within error of measurement or uniform with the exception of one or two inconclusive outliers. When larger than the size of the circle, the 95% confidence interval of the weighted mean is illustrated by a horizontal line through the circle. The fraction of all $\delta^{13}C$ analyses used in the calculation of the weighted mean is given in parentheses next to the sample number. For samples in which $\delta^{13}C$ is inhomogeneous, the range in measured values is represented by a horizontal bar. Only four samples exhibit statistically significant intracrystalline and/or grain-scale intercrystalline heterogeneity in $\delta^{13}C$.

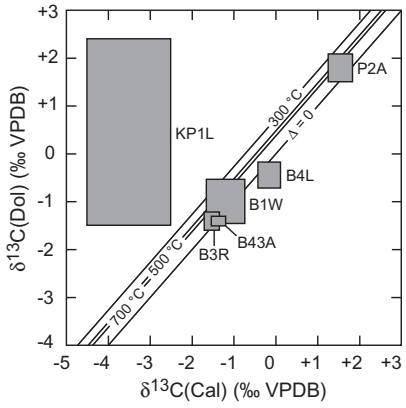

Fig. 9. Summary of all measurements of $\delta^{13}C$ in samples with coexisting calcite and dolomite. When analyses of a mineral in a sample are consistent with a uniform value or are uniform with the exception of a single inconclusive outlier, the midpoint of the corresponding side of the rectangle is the weighted mean of all but the outlying analysis and the length of the side is the 95% confidence interval of the weighted mean. When analyses of a mineral in a sample are not consistent with a uniform value, the corresponding side of the rectangle is the range in measured values. Isotherms calculated from Sheppard and Schwarcz (1970). With the exception of sample KP1L, calcite and dolomite analyses are consistent with carbon isotope exchange equilibrium or nearly so.

except for two outliers that differ from other measurements of $\delta^{18}O$ in the same grain by >6SD. Sample B4Q therefore exhibits both intercrystalline and intracrystalline heterogeneity in $\delta^{18}O$. The spatial distributions of $\delta^{18}O$ measurements in grain #5 (Fig. 2c) and #1 (not illustrated) in sample B4Q are consistent with irregular rather than concentric $\delta^{18}O$ zoning.

Minerals are homogeneous in $\delta^{18}O$ in only one of the four samples that contain a reaction front (CL29F, Fig. 11). Sample CL30A contains homogeneous calcite except for a single inconclusive outlier. Analyzed quartz is homogeneous except for three outliers that differ by >6SD in $\delta^{18}O$. None of the outlying quartz analyses, however, differ from other analyses in the same grain by >6SD. There is no significant intracrystalline or intercrystalline inhomogeneity in $\delta^{18}O$ of calcite in sample CL30A. There is intercrystalline but not intracrystalline inhomogeneity in $\delta^{18}O$ of quartz.

Oxygen isotope compositions in sample KP1L behave differently than in samples CL29F and CL30A (Fig. 11). All analyzed forsterite and calcite in the vein have homogeneous $\delta^{18}O$ both near the reaction front (Fig. 2d) and in the vein interior. In contrast, $\delta^{18}O$ of dolomite is heterogeneous with significant differences both within individual grains and between grains. Variations in $\delta^{18}O$ of dolomite are up to 9.4‰ within the same grain (Fig. 2d). The $\delta^{18}O$ zoning in dolomite in sample KP1L is irregular rather than concentric and appears related in part to variations in CL brightness and occurrences of healed fractures (Fig. 2f).

Oxygen isotope compositions in sample B43A exhibit more complicated behavior than in the other samples that contain a reaction front (Fig. 11). Dolomite is homogeneous in $\delta^{18}O$ even within 50 μm of the reaction front (Fig. 13a). Calcite adjacent to the reaction front that is filled with open pore space and small blebs of exsolved dolomite has extraordinarily variable measured $\delta^{18}O$, 3.3–15.8‰. The calcite has the same texture and isotopic heterogeneity as "turbid" calcite interpreted by Bowman et al. (2009) as the product of retrograde alteration. The measured value of $\delta^{18}O = 3.3‰$ indicates that the alteration involved fluid, at least in part, of meteoric origin, consistent with Forester and Taylor's (1977) study of meteoric hydrothermal activity on the Isle of Skye at the time of emplacement of the Beinn an Dubhaich granite. The steep gradient in $\delta^{18}O$ in turbid calcite (12.5‰ over ~100 μm, Fig. 13a) is similar to that in quartz from the Maol na Gainmhich granite, [12.7‰ (−2.9‰ to 9.8‰) over 400 μm] across microfractures that were pathways for heated meteoric water on the Isle of Skye (Valley and Graham, 1996). Further from the reaction front, calcite is "clear" (in the meaning of Bowman et al., 2009: no open pores or dolomite exsolution) and, while still inhomogeneous, is less variable in $\delta^{18}O$. A difference in $\delta^{18}O$ >6SD was measured within one clear calcite grain near the reaction front, and differences >6SD were measured between nearby calcite grains both near and away from the reaction front (Figs. 11 and 13b). Forsterite is homogeneous in $\delta^{18}O$ away from the reaction front (Fig. 13b), but nearby grains closer to the reaction front

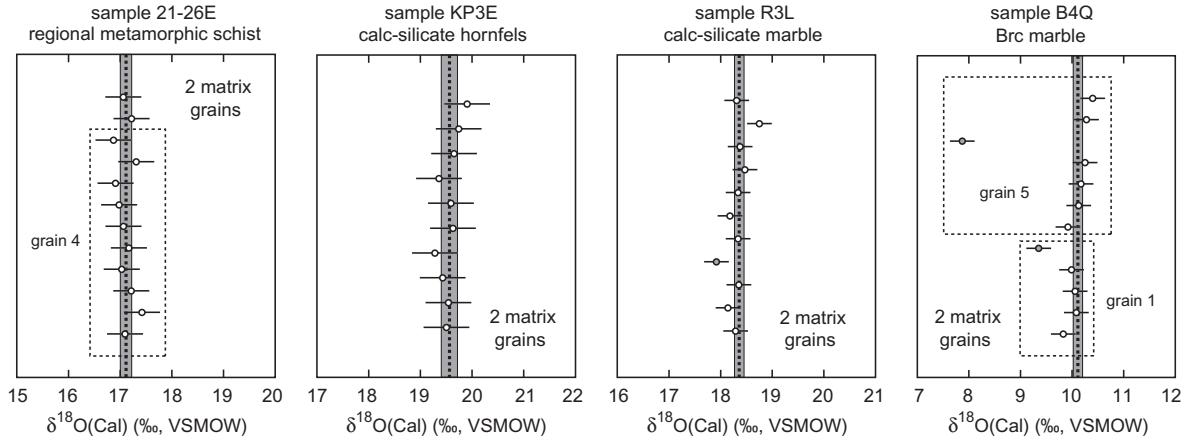

Fig. 10. All ion microprobe measurements of $\delta^{18}O$ of calcite in regional metamorphic rock, in calc-silicate hornfels and marble, and in brucite marble. Format is the same as in Fig. 4. Fig. 2a is an image of grain #4, sample 21-26E, and Fig. 2c is an image of grain #5, sample B4Q.

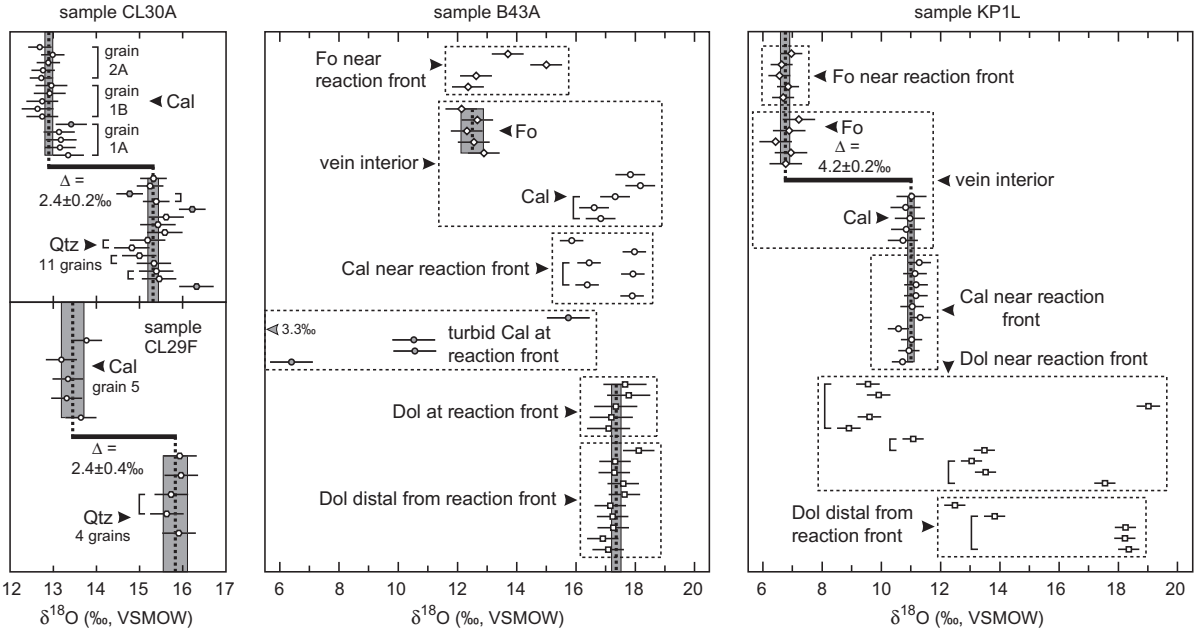

Fig. 11. All ion microprobe measurements of $\delta^{18}O$ of calcite, dolomite, quartz (Qtz), and forsterite (Fo) in samples that contain a reaction front involving Reactions (2) and (3). Format is the same as in Figs. 4, 6, and 7 except that a weighted mean was computed for $\delta^{18}O$ of quartz in sample CL30A excluding three outliers. Thick horizontal bars and number values are either $\Delta^{18}O$(Qtz–Cal) or $\Delta^{18}O$(Cal–Fo) based on the weighted mean $\delta^{18}O$ for each mineral in the sample. Calcite analyses are of "clear" calcite except for those labeled "turbid." Sites of Cal and Dol analyses in sample B43A "at reaction front" are imaged in Fig. 13a; sites of Cal and Fo analyses in the "vein interior" are imaged in Fig. 13b.

may differ by 2–3‰, a difference >6SD. Forsterite grains in sample B43A are sufficiently small that only one analysis was made per grain. Both forsterite and calcite in sample B43A therefore exhibit intercrystalline heterogeneity in $\delta^{18}O$. Intracrystalline heterogeneity in $\delta^{18}O$ was detected in calcite but was not evaluated in forsterite.

Minerals are homogeneous in $\delta^{18}O$ or nearly so in only one of the three analyzed samples that contain a pervasive distribution of reactants and products (sample B4L, Fig. 12). Forsterite is homogeneous in $\delta^{18}O$ in sample B4L, dolomite is homogeneous with the exception of a single inconclusive outlier, and calcite is homogeneous with the exception of a single outlier whose value is suspect because of its textural context (along a crack). Sample P2A, in contrast, contains dolomite that is homogeneous with the exception of two outliers, one of which is inconclusive while the other differs from four other dolomite analyses by >6SD. None of the $\delta^{18}O$ values measured in the same dolomite grain, however, differ from each other by >6SD. Analyzed calcite in sample P2A falls into two groups.

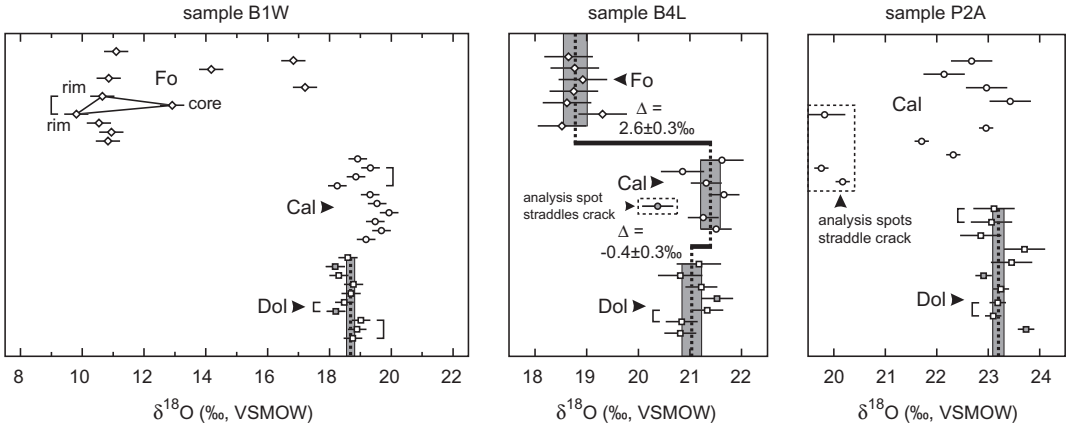

Fig. 12. All ion microprobe measurements of $\delta^{18}O$ of calcite, dolomite, and forsterite in samples that contain a pervasive distribution of reactants and products of either Reaction (1) or (3). Format is the same as in Figs. 4, 6, 7, and 11. Lower and upper thick horizontal bars and number values in the panel for sample B4L are $\Delta^{18}O$(Dol–Cal) and $\Delta^{18}O$(Cal–Fo), respectively, based on the weighted mean $\delta^{18}O$ for the two pairs of minerals. Analyses of the zoned forsterite grain in sample B1W are joined by thin solid lines; the grain itself is imaged in Fig. 2e. Because of the small grain size of the samples, most analyses are of different grains.

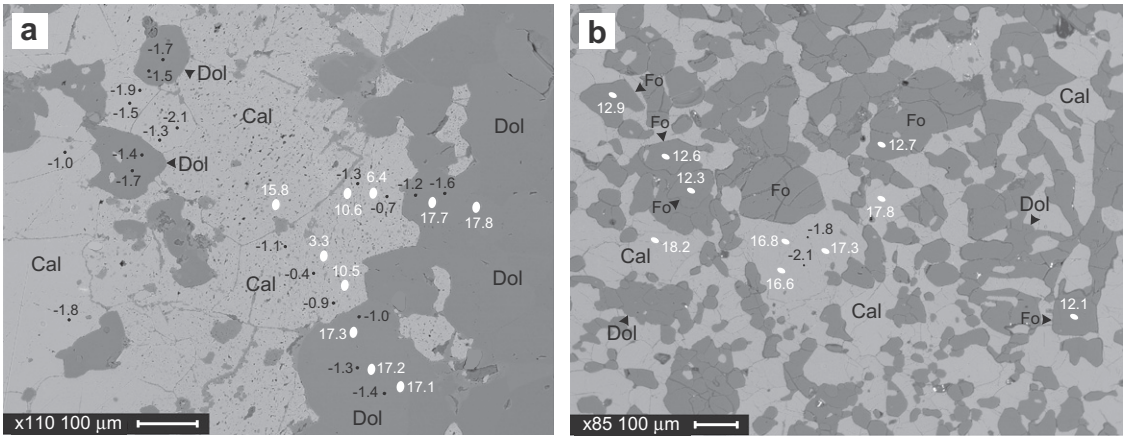

Fig. 13. BSE images of sample B43A. Format is the same as in Fig. 2. (a) Calcite at the reaction front separating dolomite from calcite + forsterite has a "turbid" texture caused by development of microporosity and dolomite exsolution blebs. Turbid calcite is uniform in $\delta^{13}C$ but highly variable in $\delta^{18}O$ (differences up to 12.5‰ over 100 μm within the field of view). White ovals are locations of $\delta^{18}O$ analyses of calcite and dolomite "at reaction front" in Fig. 11. (b) White ovals are locations of $\delta^{18}O$ analyses of calcite and forsterite in "vein interior" in Fig. 11. Clear calcite in the image has no significant microporosity or dolomite exsolution, and reduced but significant variability in $\delta^{18}O$ compared to turbid calcite. Forsterite in the vein interior has uniform $\delta^{18}O$ within error of measurement.

Analysis pits of one group, with measured $\delta^{18}O = 20–21‰$, all lie along fractures that contain BSE-dark material that in one case was thick enough to positively identify as brucite with the electron microprobe. The significance of the measured $\delta^{18}O$ values is uncertain because the values may represent calcite–brucite mixtures. The other calcite analyses are of unfractured calcite grains with values that differ by >6SD. Each calcite analysis was of a different grain. Both calcite and dolomite in sample P2A therefore exhibit intercrystalline heterogeneity in $\delta^{18}O$. Intracrystalline heterogeneity in $\delta^{18}O$, however, either was not proven (dolomite) or was not evaluated (calcite).

The behavior of oxygen isotopes in sample B1W is the most complicated of the three analyzed samples with a pervasive distribution of reactants and products (Figs. 2e and 12). Dolomite in the sample is homogeneous with the exception of two inconclusive outliers. The $\delta^{18}O$ of both calcite and forsterite differs by >6SD both within individual grains and between nearby grains. Calcite and forsterite in sample B1W therefore exhibit both intracrystalline and intercrystalline heterogeneity in $\delta^{18}O$. The range in $\delta^{18}O$ of forsterite, 7.4‰, is much larger than the range in $\delta^{18}O$ of calcite, 1.7‰.

7. DISCUSSION

7.1. Comparison of ion microprobe data with conventional analyses of isotope composition

The accuracy of the ion microprobe measurements of minerals was evaluated by comparison with values of $\delta^{18}O$ and $\delta^{13}C$ obtained by conventional phosphoric acid

or laser fluorination methods. Analyses by phosphoric acid methods were performed either in the laboratory of Douglas Rumble at the Geophysical Laboratory or in the laboratory of A.J. Kaufman at the University of Maryland; analyses by laser fluorination methods with BrF_5 as the F source were performed in the laboratory of Douglas Rumble (see references in footnote of Table 1, for analytical details). Values of $\delta^{18}O$ and $\delta^{13}C$ of calcite measured by ion microprobe were corrected for Mg content, but those measured by conventional phosphoric acid techniques were not, either because it makes no difference ($\delta^{13}C$) or the corrections were <0.1‰ ($\delta^{18}O$). All comparisons refer to the same hand specimen, but the locations of the conventional analysis and the material used for the ion microprobe mount may be as much as ~10 cm apart, and sample sizes differed by a factor of $\sim 10^6$. Only a subset of minerals in the 19 analyzed samples was considered for the following reasons. First, to compare the isotope composition of individual minerals, samples were excluded whose conventional carbonate analyses are of mixtures of calcite and dolomite (B1W, B3R, B4L, KP1B, P2A). Second, to avoid uncertainty in knowing what conventional analysis to compare with the ion microprobe data, samples with cm-scale heterogeneity in $\delta^{18}O$ and $\delta^{13}C$ based on conventional analyses were also excluded (B43A, KP1L). In the remaining samples, only those minerals were considered that either are homogeneous within error of the ion microprobe analyses or are homogeneous with the exception of no more than three outliers.

Results of the comparison for $\delta^{18}O$ and $\delta^{13}C$ are illustrated in Fig. 14. The midpoint of the vertical dimension of each box is the weighted mean value of a group of analyses by ion microprobe of a specific mineral in a particular sample. The uncertainty in the weighted mean introduced by the measurement is represented by plus or minus (±) twice the standard error (SE) of the group. The uncertainty introduced by the instrumental bias is represented by ± twice the SE of the eight bracketing standard calcite analyses. The uncertainty introduced by the isotopic composition of the standard calcite itself is represented as ± twice the SE of its composition measured by conventional phosphoric acid techniques. The total uncertainty in the composition obtained by ion microprobe, illustrated as the vertical dimension of the box, was taken as ± twice the square root of the sum of the squares of the three SEs. The midpoint of the horizontal dimension of each box is the isotopic composition of the unknown using conventional methods. The uncertainty in the measurement is taken as ± twice the SD of multiple measurements of the carbonate or silicate mineral standard in the laboratory where the measurement was made. If the measurement was made using a working standard, the uncertainty introduced by the working standard is represented by ± twice the SE of its composition measured against an international standard. The uncertainty introduced by analyses of the international standard is ± twice the SE of multiple measurements of the standard in the same laboratory. The total uncertainty in the composition obtained by conventional techniques, illustrated as the horizontal dimension of the box, was taken as ± twice the square root of the sum of the squares of the SD and two SEs (or the SD and one SE in laboratories that measure unknowns directly against an international standard).

Although the comparisons in Fig. 14 do not consider possible disagreement resulting from either the different methods of carbonate and silicate analyses or in inter-laboratory calibration, the agreement between conventional and ion microprobe analyses is very good, within error of measurement with two exceptions. One exception is $\delta^{18}O$ of quartz in sample CL29F (Fig. 14a). The disagreement between the conventional and ion microprobe analyses of quartz in sample CL29F is likely explained by small differences in $\delta^{18}O$ of quartz on the scale of the hand specimen. The other exception is $\delta^{13}C$ of calcite in sample EM10C (Fig. 14b). There probably is isotopic heterogeneity at the cm-scale in sample EM10C, as well. The datum for sample R3B in Fig. 14b just misses the 1:1 line by 0.06‰, an amount not considered significant.

7.2. Attainment and preservation of carbon and oxygen isotope exchange equilibrium

The degree to which carbon and oxygen isotope exchange equilibrium was attained and preserved at the spatial scale of the ion microprobe analyses displays great

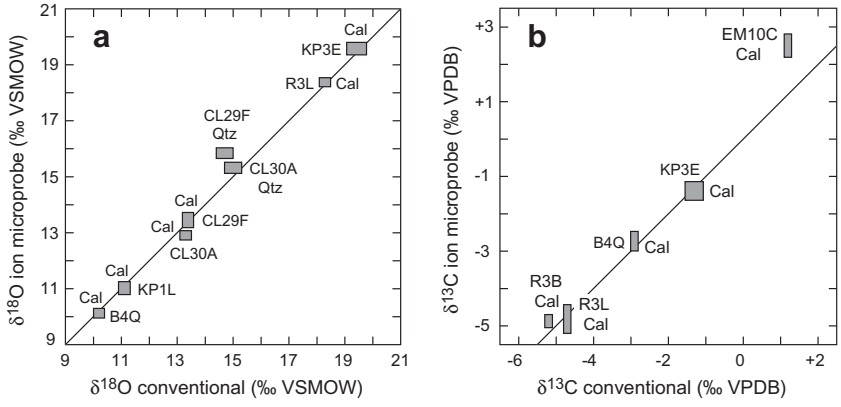

Fig. 14. Comparison of stable isotope compositions measured by ion microprobe and conventional methods for the same hand specimen. Boxes refer to the comparison of a particular mineral in a particular sample. The significance of the center and dimensions on the boxes are explained in the text. Inclined solid line represents a 1:1 relationship. (a) Comparison for $\delta^{18}O$. (b) Comparison for $\delta^{13}C$.

diversity. In four of the five samples in which both calcite and dolomite were analyzed (Figs. 11, 12, and 15a), either reactant dolomite is uniform in $\delta^{18}O$ or nearly so but product calcite is not (B1W, B43A), product calcite is uniform in $\delta^{18}O$ but reactant dolomite is not (KP1L), or both product calcite and reactant dolomite are inhomogeneous (P2A). The absence of homogeneity in $\delta^{18}O$ of calcite and/or dolomite precludes attainment and preservation of oxygen isotope exchange equilibrium between calcite and dolomite in all four samples. Sample B1W (Fig. 12) also exhibits non-equilibrium reversed oxygen isotope fractionation between calcite and dolomite (some $\delta^{18}O$ values of calcite exceed some $\delta^{18}O$ values of nearby dolomite by >6SD). Measured values of $\delta^{18}O$ in calcite and dolomite are uniform or nearly so in sample B4L (Fig. 12), and the argument against oxygen isotope equilibrium between calcite and dolomite is more involved. Both experimental and field calibrations indicate that $\Delta^{18}O(Dol–Cal) > 0$ but could be ~0 at temperatures of metamorphism (Chacko et al., 2001). If $\Delta^{18}O(Dol–Cal) \approx 0$, then the set of uniform calcite and dolomite analyses in sample B4L (open circles and squares, Fig. 12) should together be uniform within error of measurement if oxygen isotope equilibrium was attained and preserved. The MSWD = 2.41 computed from all 10 of these calcite and dolomite analyses, however, is inconsistent with a uniform composition at a 95% confidence level. Inclusion of one or both outlying calcite and dolomite analyses in sample B4L only increases the value of MSWD (to 2.68–5.35). The value of MSWD is further increased if measured calcite compositions are each corrected for a constant $\Delta^{18}O(Dol–Cal) > 0$. Measured values of $\delta^{18}O$ of calcite and dolomite therefore are not consistent with attainment and preservation of oxygen isotope exchange equilibrium in sample B4L as well.

The equilibrium value of $\Delta^{13}C(Dol–Cal)$ in the range $T = 595–710$ °C (Table 1) has not been measured experimentally but is probably ~0.3–0.4‰ (Sheppard and Schwarcz, 1970). Near-zero carbon isotope fractionation in five of the six analyzed samples with calcite and dolomite implies that calcite–dolomite carbon isotope exchange equilibrium was attained and preserved or nearly so in most samples (Figs. 6, 7, and 9). Significant departure from carbon isotope exchange equilibrium between calcite and dolomite was observed in only a single sample (KP1L, Figs. 2d, 7, and 9).

The equilibrium value of $\Delta^{18}O(Cal–Fo)$ in the range $T = 595–710$ °C (Table 1) is ~3.5–4.4‰ (Chiba et al., 1989). Accordingly, measured data are consistent with attainment and preservation of oxygen isotope exchange equilibrium between calcite and forsterite in only one sample (KP1L, Figs. 11 and 15b). In one of the other three analyzed samples with calcite and forsterite, measured $\Delta^{18}O(Cal–Fo)$ is too small (2.6±0.3‰ in sample B4L). At equilibrium, a value of $\Delta^{18}O(Cal–Fo) = 2.6±0.3$‰ corresponds to $T \approx 850 \pm 60-70$ °C (Fig. 15b), in excess of the thermal stability of dolomite observed in the sample, ~740 °C at 500 bars (Ferry et al., 2002). Calcite–forsterite oxygen isotope equilibrium is precluded in the other two samples (B1W, B43A) by the isotopic inhomogeneity in both minerals (Figs. 11, 12, and 15b). Because $\Delta^{18}O(Dol–Cal) \approx 0$ at 595–710 °C (Sheppard and Schwarcz, 1970; Chacko et al., 2001), $\Delta^{18}O(Dol–Fo) \approx 3.5–4.4$‰. Oxygen isotope exchange equilibrium between dolomite and forsterite therefore is also precluded in all four analyzed samples containing the two minerals either because of the isotopic heterogeneity of forsterite or dolomite (samples B1W, B43A, KP1L) or by the small measured $\Delta^{18}O(Dol–Fo)$ (sample B4L).

Ignoring three analyses of quartz and one of calcite with outlying $\delta^{18}O$ in sample CL30A, measured $\Delta^{18}O(Qtz–Cal)$ in samples CL29F and CL30A is the same, 2.4 ± 0.2–0.4‰ (Fig. 11). The value is significantly larger than that

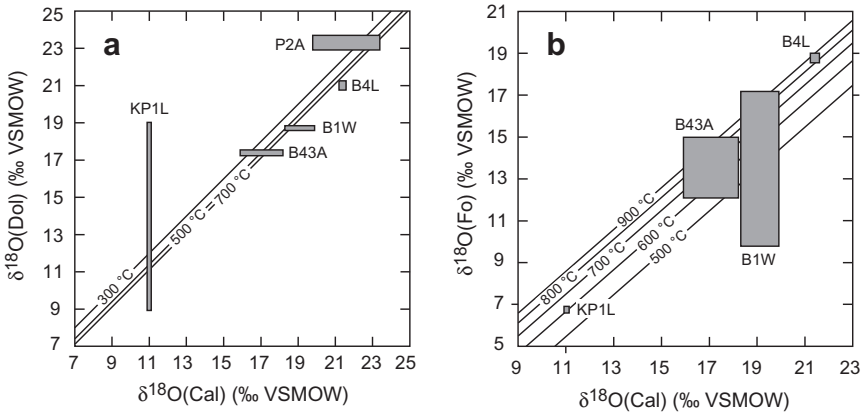

Fig. 15. Summary of all measurements of $\delta^{18}O$ in samples with coexisting calcite and dolomite (a) and calcite and forsterite (b). When analyses of a mineral in a sample are consistent with a uniform value or are uniform with the exception of one or two inconclusive outliers, the midpoint of the corresponding side of the rectangle is the weighted mean of all but the outlying analyses and the length of the side is the 95% confidence interval of the weighted mean. The weighted mean $\delta^{18}O$ of calcite in sample B4L excludes the analysis that straddles a crack (Fig. 12). When analyses of a mineral in a sample are not consistent with a uniform value, the corresponding side of the rectangle is the range in measured values. The range in $\delta^{18}O$ of calcite in sample B43A excludes analyses of turbid calcite (Fig. 11). The range in $\delta^{18}O$ of calcite in sample P2A excludes analyses that straddle a crack (Fig. 12). Isotherms in (a) are calculated from Sheppard and Schwarcz (1970); isotherms in (b) are calculated from Chiba et al. (1989). None of the analyzed calcite–dolomite pairs and only one of the analyzed calcite–forsterite pairs (sample KP1L) is consistent with oxygen isotope exchange equilibrium.

predicted by Clayton et al. (1989) for 560 °C, 0.5‰. At equilibrium, a value of $\Delta^{18}O(Qtz–Cal) = 2.4 \pm 0.4‰$ corresponds to $T < 200$ °C (Clayton et al., 1989), probably of no geological significance. Lackey and Valley (2004) measured an average $\Delta^{18}O(Qtz–Cal) = 1.8 \pm 0.3‰$ in the Mt. Morrison pendant by conventional analyses that they interpreted as evidence for oxygen isotope exchange disequilibrium between calcite and quartz. A restandardization of $\delta^{18}O$ values of calcite obtained by conventional analysis from the Mt. Morrison pendant reported by Ferry et al. (2001) (see footnote of Table 1) gives a revised value of $\Delta^{18}O(Qtz–Cal) = 1.6 \pm 0.3‰$, the same within error of measurement as that given by Lackey and Valley (2004). Quartz and calcite in samples CL29F and CL30A may never have attained oxygen isotope equilibrium during peak contact metamorphism, or equilibrium may have been attained at some point during peak metamorphism but later disturbed during retrograde metamorphism.

7.3. Survival of intracrystalline heterogeneities in carbon and oxygen isotope composition

The survival time of the observed intracrystalline heterogeneities in $\delta^{13}C$ and $\delta^{18}O$ in calcite at the conditions of metamorphism were computed to evaluate how the heterogeneities developed. Survival times at peak metamorphism and during cooling after peak metamorphism were estimated following Young and Rumble (1993), Van Haren et al. (1996), and Bowman et al. (2009). For each isotopically inhomogeneous calcite grain, the time for the maximum measured difference in $\delta^{13}C$ or $\delta^{18}O$ to be reduced by diffusion throughout the grain to $\leqslant$1SD of individual analyses was computed using Figs. 5.3 and 6.1 of Crank (1975). Calculations assume homogenization of $\delta^{13}C$ and $\delta^{18}O$ by isotope exchange at the grain margin with a medium of uniform isotope composition. Calcite grains were modeled as spheres or cylinders if they were equant or elongated, respectively. The diffusion coefficient for carbon (D_C) was calculated from the Arrhenius relationship in Labotka et al. (2000). The diffusion coefficient for oxygen (D_O) was calculated from the model of Labotka et al. (2010) that is the same as model (1a) of Kohn (1999). Diffusion coefficients at 1000 bars H_2O pressure and temperature of interest were calculated from the Arrhenius relationship in Farver (1994). The fugacity of H_2O (f_{H_2O}) at other pressures relevant to metamorphism of the samples in this study was calculated from the Kerrick and Jacobs (1981) equation of state. Peak pressure and temperature of metamorphism were taken from Table 1. As an approximation, prograde and retrograde metamorphism of the samples was considered "wet" (H_2O pressure equal to total pressure) for three reasons. First, prograde mineral reactions in all samples were driven by infiltration of rock by H_2O-rich fluids (see references in footnote of Table 1). Second, retrograde mineral reactions in contact metamorphosed carbonate rocks record continued infiltration by H_2O-rich fluids as aureoles cool (Ferry, 1996; Ferry and Rumble, 1997; Ferry et al., 1998). Third, even in the absence of a free H_2O fluid, f_{H_2O} normally corresponds more closely to "wet" than "dry" conditions as rocks cool following peak metamorphism (Kohn, 1999).

The significant intracrystalline heterogeneity in $\delta^{13}C$ but homogeneity in $\delta^{18}O$ in regional metamorphic rock sample 21-26E (grain #4, Figs. 2a, 4, and 10) was the pattern anticipated at the outset of the study. The time to reduce the 1.9‰ difference in $\delta^{13}C$ between core and rim in grain #4 to the 1SD analytical uncertainty (0.3‰) by intracrystalline diffusion at constant peak T (T_{peak}) of 500 °C is 37 My for an equant grain with radius ~135 μm (Fig. 16). The time for homogenization of an equivalent difference in $\delta^{18}O$ is 1100 years. The time that the measured difference in $\delta^{13}C$ in grain #4 could survive linear cooling from peak temperature was calculated using the same analysis by replacing the value of D_C for $T_{peak} = 500$ °C with a temperature-average value ($\overline{D}$) between 200 °C and T_{peak}, calculated from:

$$\overline{D} = \left[\int_{200}^{T_{peak}} D(T)dT\right] \Big/ (T_{peak} - 200) \quad (4)$$

Because $D(T)$ follows an Arrhenius relationship, the exact value of the lower limit on temperature is unimportant. The calculated time is 390 My (Fig. 16). Calculated times of 37 and 390 My are longer than the duration of peak regional metamorphism and entire cycles of regional metamorphism, respectively, while 1100 years is much shorter than either (England and Thompson, 1984; Lyubetskaya and Ague, 2009). It was expected therefore that carbon isotope zonation would develop in calcite grains at or near T_{peak} during regional metamorphism and be preserved during cooling while oxygen isotope zonation would not. The concentric $\delta^{13}C$ zoning illustrated in Fig. 2a with values decreasing by up to ~2‰ between core (maximum $\delta^{13}C = -9.0‰$) and rim (minimum $\delta^{13}C = -10.9‰$) is the same in magnitude as the ^{13}C depletion predicted from metamorphic decarbonation reactions (Valley, 1986; Nabelek, 1991; Baumgartner and Valley, 2001). The sim-

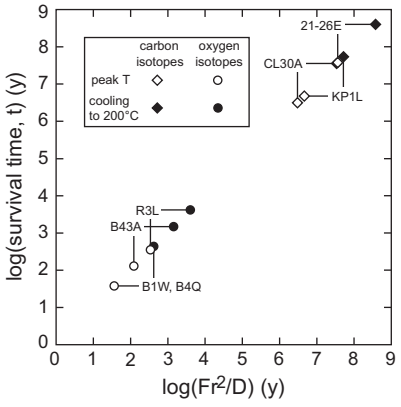

Fig. 16. Calculated survival time (t) of isotopic zoning in calcite grains [r is grain radius, D is the diffusion coefficient for O or C, and F is the non-dimensional number Dt/r^2 for when diffusion has homogenized $\delta^{18}O$ (circles) or $\delta^{13}C$ (diamonds) to the extent that variations throughout the grain are $\leqslant$1SD of the measurement error (see text for details)]. Calculations are for both survival time at peak temperature (open symbols) and following linear cooling to 200 °C (filled symbols).

plest interpretation of the $\delta^{13}C$ zonation illustrated in Fig. 2a is that it was produced by carbon isotope fractionation during prograde decarbonation reactions during regional metamorphism. Because of relatively rapid oxygen diffusion, associated zonation in $\delta^{18}O$ either never developed or was erased by diffusion during cooling.

Calcite grains with heterogeneous $\delta^{13}C$ and homogeneous $\delta^{18}O$ in the forsterite–calcite vein from the Twin Lakes pendant (sample KP1L, Figs. 2d, 7, and 11) and in sample CL30A from the Mt. Morrison pendant (Figs. 7 and 11) can be explained similarly. At $T_{peak} \approx 595$ °C for sample KP1L, the calculated survival time of the 1.7‰ difference in $\delta^{13}C$ within the large calcite grain at the reaction front (Figs. 2d and 7) is 4.7 My, and its survival time during linear cooling to 200 °C is 53 My (Fig. 16). At $T_{peak} \approx 560$ °C for sample CL30A, the calculated survival time of the 1.9‰ difference in $\delta^{13}C$ within grain #8 (Fig. 7) is 3.1 My, and its survival time during linear cooling to 200 °C is 35 My (Fig. 16). Both times for the two samples are longer than typical episodes of contact metamorphism around a single pluton (Furlong et al., 1991; Cook et al., 1997; Nabelek, 2009). The survival time of an equivalent 1.7‰ and 1.9‰ difference in $\delta^{18}O$ at T_{peak} is ~900 years for the large calcite grain in sample KP1L and ~740 years for grain #8 in sample CL30A, less than the duration that temperature remains near peak values during contact metamorphism. Values of $\delta^{13}C$ of calcite in sample KP1L in Fig. 2d are up to 6–7‰ less than that of unaltered reactant dolomite (Fig. 7). Values of $\delta^{13}C$ of calcite in sample CL30A in Fig. 7 are up to ~2‰ less than that in calcite–quartz rocks without wollastonite further from the reaction front (−0.9‰ to −0.8‰, Table 4, Ferry et al., 2001). The simplest explanation of $\delta^{13}C$ zonation exhibited in samples KP1L and CL30A, therefore, is carbon isotope fractionation during prograde decarbonation Reactions (2) and (3) and, in the case of sample KP1L, additional isotope exchange with a low-$\delta^{13}C$ infiltrating fluid. Because of relatively rapid oxygen isotope diffusion, associated zonation of $\delta^{18}O$ in calcite either never developed during contact metamorphism or was erased by diffusion during cooling.

The pattern of isotope heterogeneities in samples B1W, B4Q, and B43A from the Beinn an Dubhaich aureole and in sample R3L from the Ritter Range pendant, on the other hand, are the opposite of expectations. Values of $\delta^{13}C$ within individual calcite grains are uniform or nearly so but values of $\delta^{18}O$ can display significant heterogeneity (Figs. 2, 5–7, and 10–12). The calculated survival time of the measured $\delta^{18}O$ zonation in calcite grains from the three samples from the Beinn an Dubhaich aureole at peak temperature and during linear cooling to 200 °C are all ~40–130 years and ~430–1500 years, respectively (Fig. 16). The corresponding times for the sample from the Ritter Range pendant are ~350 and ~4100 years (Fig. 16). The duration of episodes of contact metamorphism is much longer than 430–4100 years and temperature persists near peak values for longer than 40–350 years. The intracrystalline heterogeneities in $\delta^{18}O$ in the four samples therefore must have been produced during retrograde metamorphism. An upper bound on the temperature at which the $\delta^{18}O$ zonation developed can be estimated as the maximum temperature below which measured differences in isotopic composition within grains cannot be reduced by diffusion to the 1SD analytical uncertainty during linear cooling to 200 °C over 100 ky. Values of $\overline{D}_O$ for the cooling interval were computed from Eq. (4). Upper bounds for all samples are in the range 485–510 °C, and they lie within the temperature interval, 355–595 °C, over which periclase was altered to brucite, forsterite was altered to serpentine, and wollastonite was altered to calcite + quartz as aqueous fluids flowed through the aureoles while they cooled (Ferry and Rumble, 1997; Ferry et al., 1998). If the duration of cooling to 200 °C was 50 ky, calculated temperatures are raised by 20–25 °C. If the duration of cooling to 200 °C was longer than 100 ky, calculated temperatures are lower. The simplest explanation of intracrystalline $\delta^{18}O$ zonation in calcite in the four samples is partial oxygen isotope exchange between rock and reactive fluids that flowed through the aureoles after they cooled below peak temperatures. Diffusive exchange of minerals with late retrograde fluids also was proposed to have caused smooth $\delta^{18}O$ gradients of 10‰ over 200 μm in calcite and of 9‰ over 10 μm in magnetite from granulite facies marbles elsewhere (Wada, 1988; Valley and Graham, 1991; Graham et al., 1998; Valley, 2001). Where retrograde alteration is extensive, altered calcite adopts a turbid texture, and extreme gradients in $\delta^{18}O$ develop, >10‰ over distances of ~100 μm (Fig. 13a). These gradients, however, do not appear smooth and may be controlled by fine-scale porosity or unseen microcracks rather than by intracrystalline diffusion. The absence of any associated alteration of $\delta^{13}C$ (also reposted by Wada (1988)) can be explained by the low X_{CO_2} of fluids involved in reactions that produced brucite, serpentine, and quartz (Ferry and Rumble, 1997; Ferry et al., 1998).

7.4. Overview of observed heterogeneity in carbon and oxygen isotope composition

7.4.1. Correlation of isotope heterogeneity with petrologic context

Measured degrees of grain-scale heterogeneity in $\delta^{13}C$ and $\delta^{18}O$ systematically differ depending on petrologic context. Calcite in regional metamorphic rock, calc-silicate hornfels and marble, and brucite marble, with few exceptions, lacks evidence for extensive inhomogeneity in either $\delta^{18}O$ or $\delta^{13}C$. Among the 11 samples in these groups, only a single one contains calcite with inhomogeneous $\delta^{13}C$ (21-26E). Calcite in the other 10 samples is either homogeneous or homogeneous with the exception of one or two inconclusive outliers (Fig. 8). Among the four out of these 11 samples analyzed for oxygen isotope composition (Fig. 17a), two contain calcite that is homogeneous in $\delta^{18}O$ (21-26E, KP3E). Heterogeneity in $\delta^{18}O$ of calcite in the other two samples is defined by either just one (R3L) or two (B4Q) outliers in populations of otherwise homogeneous $\delta^{18}O$ values (Fig. 10).

In contrast, measured $\delta^{18}O$ and/or $\delta^{13}C$ values are inhomogeneous in six of the eight samples containing either a reaction front or a pervasive distribution of reactants and products (Figs. 6–9, 11, 12, 15, and 17). The two exceptions are samples B3R and B4L. The behavior in carbon and

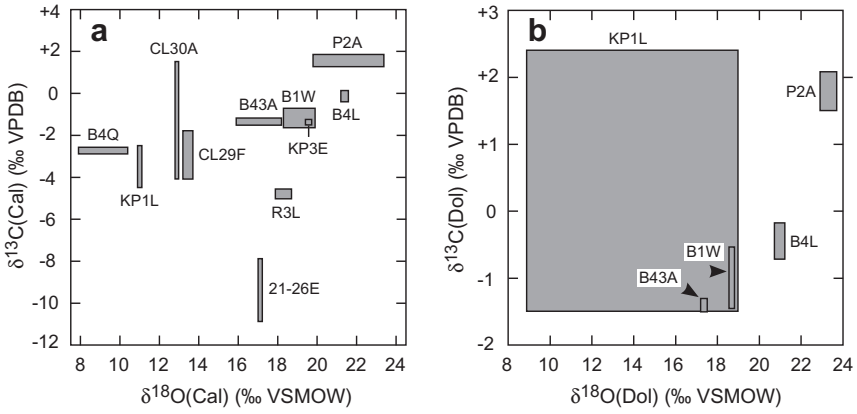

Fig. 17. Summary of all $\delta^{18}O$ and $\delta^{13}C$ analyses of calcite (a) and dolomite (b) from the same sample. Format is the same as in Figs. 9 and 15. All different combinations of isotope behavior are observed: both $\delta^{18}O$ and $\delta^{13}C$ are homogeneous within error of measurement (e.g., dolomite in sample B43A), both $\delta^{18}O$ and $\delta^{13}C$ are inhomogeneous (e.g., dolomite in sample KP1L), $\delta^{18}O$ is homogeneous but $\delta^{13}C$ is not (e.g., calcite in sample 21-26E), and $\delta^{13}C$ is homogeneous but $\delta^{18}O$ is not (e.g., calcite in sample P2A).

oxygen isotope compositions in the six heterogeneous samples displays remarkable diversity. Heterogeneity in $\delta^{13}C$ is limited to the samples that contain a reaction front. The $\delta^{13}C$ of dolomite is inhomogeneous in only one (KP1L) while $\delta^{13}C$ of calcite is inhomogeneous in three (CL29F, CL30A, KP1L) (Figs. 8 and 17b). Heterogeneity of $\delta^{18}O$ in one or more minerals is more common. The $\delta^{18}O$ of dolomite is inhomogeneous in two samples (KP1L, P2A) while $\delta^{18}O$ of calcite is inhomogeneous in three (B1W, B43A, P2A) (Figs. 11, 12, and 17a). Among the four samples with analyzed forsterite, two contain forsterite with inhomogeneous $\delta^{18}O$ (B1W, B43A) (Fig. 15b). One of the two samples with analyzed quartz contains quartz with inhomogeneous $\delta^{18}O$ (Fig. 11).

7.4.2. Systematic difference in behavior between $\delta^{13}C$ and $\delta^{18}O$

Only four of the 19 analyzed samples exhibit significant grain-scale heterogeneity in $\delta^{13}C$ (Fig. 8). All 19 samples contain products of decarbonation reactions such as diopside, wollastonite, forsterite, and brucite (after periclase). Because of the fractionation of carbon isotopes between carbonate minerals and CO_2, grain-scale variations in $\delta^{13}C$ should have developed in all samples. Calculated survival times indicate that these variations, once formed, would resist homogenization by intracrystalline diffusion during metamorphism and subsequent cooling. The general absence of grain-scale heterogeneity in $\delta^{13}C$ therefore implies that the heterogeneity was erased by some process other than diffusion. The process likely was recrystallization, as argued by Bowman et al. (2009) for rocks from the Alta aureole that are similar to the brucite marbles of this study. More extensive recrystallization of samples in which prograde decarbonation reaction had gone to completion may also explain their greater isotopic homogeneity than samples that retain reactants and products. The cause of this difference in behavior, however, is not understood.

In contrast, 9 of 11 analyzed samples exhibit either grain-scale heterogeneity in $\delta^{18}O$, non-equilibrium oxygen isotope fractionations, or both (Figs. 10–12, 15, and 17). Calculated survival times indicate that intracrystalline diffusion would have erased the inhomogeneities in calcite at or during cooling from peak temperature. The $\delta^{18}O$ heterogeneity therefore must have developed during retrograde metamorphism. Stable isotope alteration appears to have occurred in a chronology of three stages following peak metamorphism. First, recrystallization erased intercrystalline and intracrystalline variations in $\delta^{13}C$ in most samples. Recrystallization would have erased any variations in $\delta^{18}O$, if they existed, as well. Second, partial isotope exchange of rocks with CO_2-poor fluids during later retrograde metamorphism caused variations in $\delta^{18}O$ of calcite of up to several per mil without affecting $\delta^{13}C$ or causing turbidity. A third stage occurred in sample B43A (and in samples described by Bowman et al. (2009)) when further fluid–rock interaction transformed clear calcite with grain-scale variations in $\delta^{18}O$ of no more than several per mil into turbid calcite with variations in $\delta^{18}O$ up to 12‰. The few occurrences of grain-scale variation in $\delta^{13}C$ and the more common occurrence of grain-scale variation in $\delta^{18}O$, as well as the chronology of isotope alteration that they imply, raise a concern over how much measured stable isotope compositions represent the $\delta^{13}C$ and $\delta^{18}O$ of carbonate minerals during mineral reaction at or near peak temperature. As a corollary, however, these results suggest that multiple late fluid events may now be understood through more detailed studies.

7.4.3. No correlation between isotopic heterogeneity of a mineral and heterogeneity in other minerals in the sample

Grain-scale isotopic inhomogeneity of one mineral in a sample correlates poorly with inhomogeneity in other analyzed minerals. For example, sample KP1L contains dolomite that is inhomogeneous in $\delta^{18}O$ while forsterite and calcite are homogeneous (Figs. 11 and 15). Sample B1W displays the opposite behavior with inhomogeneous calcite and forsterite but dolomite that is homogeneous except for two inconclusive outliers (Figs. 12 and 15). Many other combinations of homogeneous and inhomogeneous minerals were also observed in other samples (Figs. 4–12, 15, and 17).

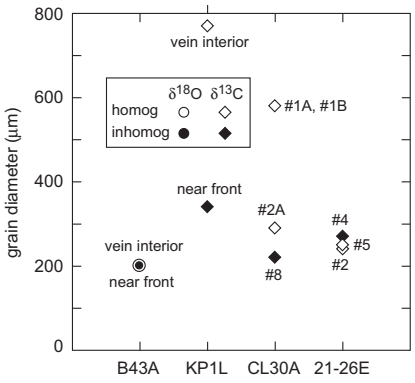

Fig. 18. Measured relationship between grain size and isotopic homogeneity of calcite in four analyzed samples. With one exception, grain diameter was measured along the traverse on which analyses were made. In the case of the exception, grain #4, sample 21-26E (Fig. 2a), that is covered with analysis points, diameter was measured as the narrowest grain width. Grain designations are the same as those in Figs. 4, 7, and 11. There is no indication that inhomogeneous grains are systematically larger grains.

7.4.4. No correlation between heterogeneity in $\delta^{13}C$ and $\delta^{18}O$ in the same mineral in a sample

Likewise, grain-scale inhomogeneities in $\delta^{18}O$ and $\delta^{13}C$ in the same mineral in the same sample are poorly correlated. Four samples contain calcite that is inhomogeneous in $\delta^{13}C$ but homogeneous in $\delta^{18}O$ or homogeneous with the exception of a single inconclusive outlier (21-26E, CL29F, CL30A, KP1L) (Fig. 17a). On the other hand, five samples contain calcite that is inhomogeneous in $\delta^{18}O$ but homogeneous in $\delta^{13}C$ or homogeneous with the exception of a single inconclusive outlier (B1W, B4Q, B43A, P2A, R3L) (Figs. 5–12 and 17a). Likewise, dolomite in sample P2A is inhomogeneous in $\delta^{18}O$ but homogeneous in $\delta^{13}C$ (Fig. 17b). There is only a single mineral in a single sample that is inhomogeneous in both $\delta^{13}C$ and $\delta^{18}O$ (dolomite in sample KP1L) (Fig. 17b).

7.4.5. No correlation between intracrystalline isotopic heterogeneity and grain size

Four of the analyzed samples contain both homogeneous and inhomogeneous calcite grains that allow evaluation of whether there is a correlation between intracrystalline heterogeneity and grain size. The possible correlation can be evaluated for $\delta^{18}O$ in one sample (B43A) and for $\delta^{13}C$ in the other three (KP1L, CL30A, 21-26E). Results are illustrated in Fig. 18. There is no indication that smaller grains are more homogeneous than larger ones. Inhomogeneous grains are either smaller than or approximately the same size as homogeneous grains in the same sample.

7.5. Implications for applications of stable isotope geochemistry to metamorphic petrology

One of the goals of the study was to better understand how stable isotopes are redistributed during metamorphic mineral–fluid reactions. Models of the redistribution process normally assume that minerals are homogeneous in $\delta^{13}C$ and $\delta^{18}O$, that there are no grain-to-grain variations in $\delta^{13}C$ and $\delta^{18}O$, and that minerals are in carbon and oxygen isotope exchange equilibrium during reaction (e.g., Rumble, 1982; Chamberlain et al., 1990). Alternative approaches have considered either that product phases but not reactants are in isotope exchange equilibrium (Müller et al., 2004), or that only carbonate minerals equilibrate with fluid (Lattanzi et al., 1980). Results of this study provide a direct test of which, if any, of these assumptions is generally correct. While $\delta^{13}C$ and $\delta^{18}O$ are uniform or nearly so both within and between nearby grains in some samples, there are many exceptions to each of these assumptions (Figs. 4–7 and 10–12). Among analyzed samples with reactants and products of a metamorphic mineral reaction, reactant minerals may be homogeneous or nearly so in both $\delta^{13}C$ and $\delta^{18}O$ (e.g., dolomite in sample B4L; Figs. 6 and 12) or in neither (e.g., dolomite in sample KP1L; Figs. 7 and 11). Product minerals may be homogenous or nearly so in both $\delta^{13}C$ and $\delta^{18}O$ (e.g., calcite in sample B4L; Figs. 6 and 12), inhomogeneous in $\delta^{13}C$ but not in $\delta^{18}O$ (e.g., calcite in sample KP1L; Figs. 7 and 11), or inhomogeneous in $\delta^{18}O$ but not in $\delta^{13}C$ (e.g., calcite in sample B1W; Figs. 6 and 12). Grain-to-grain variations in $\delta^{13}C$ and $\delta^{18}O$ of reactant minerals may be present (e.g., calcite and quartz in sample CL30A; Figs. 7 and 11) or not (e.g., dolomite in sample B43A; Figs. 7 and 11). Grain-to-grain variations in $\delta^{18}O$ of product minerals can be present (e.g., calcite and forsterite in sample B1W; Fig. 12) or not (e.g., calcite and fosterite in sample KP1L; Fig. 11). Mineral reactants may not be in oxygen isotope equilibrium with each other (e.g., calcite and quartz in samples CL29F, CL30A; Fig. 11). Mineral products can be in oxygen isotope equilibrium with each other (e.g., calcite and forsterite in sample KP1L; Fig. 11) or not (e.g., calcite and forsterite in sample B1W; Fig. 12). There are no analyzed samples in which reactants and products are in oxygen isotope equilibrium with each other (e.g., calcite + dolomite ± forsterite in samples B1W, B4L, B43A, KP1L, P2A; Figs. 11 and 12). Mineral reactants and products, however, can be in carbon if not oxygen isotope equilibrium with each other (e.g., calcite and dolomite in sample P2A; Figs. 6 and 12). None of the different sets of simple assumptions about stable isotope homogeneity and equilibration in metamorphic rocks therefore is generally valid, and none, in fact, apply to any of the individual samples analyzed in the study.

The carbon and oxygen isotope compositions of minerals provide insight into numerous other aspects of the process of metamorphism. The fractionation of carbon and oxygen isotopes between coexisting minerals is the basis for isotope thermometry (Valley, 2001). If the temperature of mineral–fluid equilibrium can be estimated and mineral–fluid isotope fractionations are known, the $\delta^{13}C$ and $\delta^{18}O$ of minerals record the carbon and oxygen isotope compositions of coexisting metamorphic fluid (Valley, 1986; Nabelek, 1991; Wing and Ferry, 2007). Profiles in $\delta^{13}C$ and/or $\delta^{18}O$ of a mineral across the contact between two lithologies with differing initial isotopic compositions quantitatively constrain the distance of intergranular diffusion during metamorphism and the relative importance of advection and diffusion in isotope

transport across the contact (Bickle and Baker, 1990; Cartwright and Valley, 1991; Bickle et al., 1997; Ferry et al., 2001). If profiles across the lithologic contact are measured for both $\delta^{13}C$ and $\delta^{18}O$, the difference in carbon and oxygen isotope diffusion distances records the X_{CO_2} of metamorphic fluid (Bickle et al., 1997; Roselle et al., 1999; Baumgartner and Valley, 2001; Müller et al., 2009). Plots of $\delta^{13}C$ against $\delta^{18}O$ for suites of metamorphic rocks that have experienced variable degrees of decarbonation reaction can distinguish open-system behavior (volatile loss accompanied by infiltration) from closed-system behavior (volatile loss without infiltration) as well as the mechanism of volatile loss (batch devolatilization versus Rayleigh distillation) (Valley, 1986; Nabelek, 1991; Baumgartner and Valley, 2001). For each of these applications to be successful, results of this study demonstrate that the intercrystalline and intracrystalline homogeneity in stable isotope composition and the approach to isotope exchange equilibrium among minerals may need to be evaluated in greater detail than has been possible in the past. In addition, the degree to which measured isotopic compositions are the same as those when minerals experienced mineral reactions near or at peak temperature should be carefully considered.

7.6. Prediction of grain-scale variability in carbon and oxygen isotope composition

The investigation points to five different indications that a sample may exhibit intracrystalline and/or grain-scale intercrystalline heterogeneity in $\delta^{13}C$ or $\delta^{18}O$ or both. First, both samples in this study that exhibit cm-scale bulk heterogeneity in $\delta^{18}O$ (samples KP1L and B43A, Fig. 3) display intracrystalline and grain-scale intercrystalline heterogeneity in $\delta^{18}O$ as well. The correlation, however, is not universal. Bowman et al. (2009) describe contact metamorphosed marbles that display cm-scale but not significant intracrystalline heterogeneity in $\delta^{18}O$. Likewise, variation in bulk $\delta^{13}C$ at the cm-scale may correlate with intracrystalline and grain-scale intercrystalline heterogeneity in $\delta^{13}C$ (sample KP1L) or not (sample B43A). Second, turbid calcite, in all samples examined to date, has highly variable $\delta^{18}O$ (Figs. 11 and 13a), apparently related to retrograde fluid–rock reaction (this study; Bowman et al., 2009). Third, all but one of the samples in this study with coexisting reactants and products of an arrested metamorphic devolatilization reaction also contain one or more minerals that exhibit intracrystalline or grain-scale intercrystalline heterogeneities in $\delta^{13}C$ or $\delta^{18}O$ or both. The exception, sample B4L (Figs. 6 and 12), demonstrates that this indicator, however, is not foolproof. Fourth, mottling observed in CL at a microscopic scale can be correlated spatially with intracrystalline heterogeneity in $\delta^{13}C$ and $\delta^{18}O$ at the same scale (Fig. 2f; Graham et al., 1998; Lewis et al., 1998). Many other samples investigated in this study, on the other hand, display intercrystalline and intracrystalline heterogeneities in $\delta^{13}C$ and/or $\delta^{18}O$, yet exhibit nothing unusual in their appearance in CL. Finally, rounded forsterite crystal morphology in contact metamorphosed dolomite marbles (e.g., samples B1W and B43A; Figs. 2e and 13b) indicates forsterite produced by a mineral reaction that proceeded far from equilibrium (Roselle et al., 1997). Mineral reaction at far from equilibrium conditions apparently results in a disequilibrium distribution of oxygen isotopes among product minerals with consequent intracrystalline and intercrystalline heterogeneity in $\delta^{18}O$ (samples B1W and B43A; Figs. 11 and 12).

Given the diversity in stable isotope inhomogeneity both within grains and between nearby grains and the common departure from oxygen isotope exchange equilibrium among coexisting minerals observed in this study, there appears to be no substitute for ion microprobe analysis in the identification and characterization of grain-scale isotope heterogeneity in metamorphic rocks. Continued studies with the latest generation of SIMS instruments dedicated to stable isotope analysis promise a new level of understanding of how stable isotope compositions best can be used to decode metamorphic process. Improved imaging and element mapping will be an important complement to these studies, allowing in situ measurements to be placed in context with textures and zoning. Correlations among textures, element zoning, and stable isotope variations, in turn, promise to reveal much new information about reaction kinetics, reactive fluid flow, and thermal histories during metamorphism.

ACKNOWLEDGMENTS

National Science Foundation (NSF) Grant EAR-0509639 and Department of Energy Grant 93ER14389 to J.W.V. and NSF Grant EAR-0635608 to J.M.F. are gratefully acknowledged. The WiscSIMS Ion Microprobe laboratory is partly supported by NSF Grants EAR-0319230, 0516725, and 0744079 and by the University of Wisconsin-Madison. J.M.F. was assisted by John Fournelle in use of the SEM for BSE and CL imaging and by Sorena Sorensen in use of the Luminoscope for CL imaging. Brian Hess masterfully polished the ion microprobe mounts, and Jim Kern and Reinhart Kozdon assisted in numerous ways with sample preparation and the ion microprobe analyses. The authors thank A.J. Kaufman for providing access to his laboratory at the University of Maryland and Jay Ague, John Bowman, and Peter Nabelek for their patient and thoughtful reviews.

APPENDIX A. SUPPLEMENTARY DATA

Supplementary data associated with this article can be found, in the online version, at doi:10.1016/j.gca.2010.08.039.

REFERENCES

Baumgartner L. P. and Valley J. W. (2001) Stable isotope transport and contact metamorphic fluid flow. In *Stable Isotope Geochemistry*, vol. 43 (eds. J. W. Valley and D. R. Cole). *Rev. Mineral. Geochem.* pp. 415–468.

Bickle M. J. and Baker J. (1990) Advective diffusive transport of isotopic fronts: an example from Naxos, Greece. *Earth Planet. Sci. Lett.* **97**, 78–93.

Bickle M. J., Chapman H. J., Ferry J. M., Rumble D. and Fallick A. E. (1997) Fluid flow and diffusion in the Waterville limestone, south-central Maine: constraints from strontium, oxygen, and carbon isotope profiles. *J. Petrol.* **38**, 1489–1512.

Bowman J. R. (1998) Stable-isotope systematics in skarns. In *Mineralized Intrusion-related Skarn Systems*, vol. 26 (ed. D. R. Lentz). *Mineral. Assoc. Canada Short Course Series*. pp. 99–146.

Bowman J. R., Valley J. W. and Kita N. T. (2009) Mechanisms of oxygen isotopic exchange and isotopic evolution of $^{18}O/^{16}O$-depleted periclase zone marbles in the Alta aureole, Utah: insights from ion microprobe analysis of calcite. *Contrib. Mineral. Petrol.* **157**, 77–93.

Cartwright I. and Valley J. W. (1991) Steep oxygen-isotope gradients at marble–metagranite contacts in the Northwest Adirondack Mountains, New York, USA: products of fluid-hosted diffusion. *Earth Planet. Sci. Lett.* **107**, 148–163.

Chacko T., Cole D. R. and Horita J. (2001) Equilibrium oxygen, hydrogen, and carbon isotope fractionation factors applicable to geologic systems. In *Stable Isotope Geochemistry*, vol. 43 (eds. J. W. Valley and D. R. Cole). *Rev. Mineral. Geochem.* pp. 1–81.

Chamberlain C. P. and Conrad M. E. (1991) Oxygen isotope zoning in garnet. *Science* **254**, 403–406.

Chamberlain C. P. and Conrad M. E. (1993) Oxygen isotope zoning in garnet: a record of volatile transport. *Geochim. Cosmochim. Acta* **57**, 2613–2629.

Chamberlain C. P., Ferry J. M. and Rumble D. (1990) The effect of net-transfer reactions on the isotopic composition of minerals. *Contrib. Mineral. Petrol.* **105**, 322–336.

Chiba H., Chacko T., Clayton R. N. and Goldsmith J. R. (1989) Oxygen isotope fractionations involving diopside, forsterite, magnetite, and calcite. *Geochim. Cosmochim. Acta* **53**, 2985–2995.

Clayton R. N., Goldsmith J. R. and Mayeda T. K. (1989) Oxygen isotope fractionation in quartz, albite, anorthite, and calcite. *Geochim. Cosmochim. Acta* **53**, 725–733.

Cook S. J., Bowman J. R. and Forster C. B. (1997) Contact metamorphism surrounding the Alta stock: finite element simulation of heat- and $^{18}O/^{16}O$ mass-transport during prograde metamorphism. *Am. J. Sci.* **297**, 1–55.

Crank J. (1975) *The Mathematics of Diffusion*. Oxford University Press, Oxford.

Davis S. R. and Ferry J. M. (1993) Fluid infiltration during contact metamorphism of interbedded marble and calc-silicate hornfels, Twin Lakes area, central Sierra Nevada, California. *J. Metamorph. Geol.* **11**, 71–88.

Eiler J. M., Valley J. W., Graham C. M. and Baumgartner L. P. (1995a) Ion microprobe evidence for the mechanisms of stable-isotope retrogression in high-grade metamorphic rocks. *Contrib. Mineral. Petrol.* **118**, 365–378.

Eiler J. M., Valley J. W., Graham C. M. and Baumgartner L. P. (1995b) The oxygen isotope anatomy of a slowly cooled metamorphic rock. *Am. Mineral.* **80**, 757–764.

England P. C. and Thompson A. B. (1984) Pressure–temperature–time paths of regional metamorphism. I: Heat transfer during evolution of regions of thickened continental crust. *J. Petrol.* **25**, 894–928.

Farver J. R. (1994) Oxygen self-diffusion in calcite: dependence on temperature and water fugacity. *Earth Planet. Sci. Lett.* **121**, 575–587.

Ferry J. M. (1988) Infiltration-driven metamorphism in northern New England, USA. *J. Petrol.* **29**, 1121–1159.

Ferry J. M. (1994) Overview of the petrologic record of fluid flow during regional metamorphism in northern New England. *Am. J. Sci.* **294**, 905–988.

Ferry J. M. (1996) Prograde and retrograde fluid flow during contact metamorphism of siliceous carbonate rocks from the Ballachulish aureole, Scotland. *Contrib. Mineral. Petrol.* **124**, 235–254.

Ferry J. M. and Rumble, III, D. (1997) Formation and destruction of periclase by fluid flow in two contact aureoles. *Contrib. Mineral. Petrol.* **128**, 313–334.

Ferry J. M., Sorensen S. S. and Rumble, III, D. (1998) Structurally controlled fluid flow during contact metamorphism in the Ritter Range pendant, California, USA. *Contrib. Mineral. Petrol.* **130**, 358–378.

Ferry J. M., Wing B. A. and Rumble, III, D. (2001) Formation of wollastonite by chemically reactive fluid flow during contact metamorphism, Mt. Morrison pendant, Sierra Nevada, California, USA. *J. Petrol.* **42**, 1705–1728.

Ferry J. M., Wing B. A., Penniston-Dorland S. C. and Rumble, III, D. (2002) The direction of fluid flow during contact metamorphism of siliceous carbonate rocks: new data from the Monzoni and Predazzo aureoles, northern Italy, and a global review. *Contrib. Mineral. Petrol.* **142**, 679–699.

Forester R. W. and Taylor, Jr., H. P. (1977) $^{18}O/^{16}O$, D/H, and $^{13}C/^{12}C$ studies of the Tertiary igneous complex of Skye, Scotland. *Am. J. Sci.* **277**, 136–177.

Furlong K. P., Hanson R. B. and Bowers J. R. (1991) Modeling thermal regimes. In *Contact Metamorphism*, vol. 26 (ed. D. M. Kerrick). *Rev. Mineral.* pp. 437–505.

Graham C. M., Valley J. W., Eiler J. M. and Wada H. (1998) Timescales and mechanisms of fluid infiltration in marble: an ion microprobe study. *Contrib. Mineral. Petrol.* **132**, 371–389.

Jamtveit B. and Hervig R. L. (1994) Constraints on transport and kinetics in hydrothermal systems from zoned garnet crystals. *Science* **263**, 505–508.

Kelly J. L., Fu B., Kita N. T. and Valley J. W. (2007) Optically continuous silcrete cements of the St. Peter sandstone: oxygen isotope analysis by ion microprobe and laser fluorination. *Geochim. Cosmochim. Acta* **71**, 3812–3832.

Kerrick D. M. and Jacobs G. K. (1981) A modified Redlich–Kwong equation for H_2O, CO_2, and H_2O–CO_2 mixtures at elevated pressures and temperatures. *Am. J. Sci.* **281**, 735–767.

Kita N. T., Ushikubo T., Fu B. and Valley J. W. (2009) High precision SIMS oxygen isotope analyses and the effect of sample topography. *Chem. Geol.* **264**, 43–57.

Kita N. T., Nagahara H., Tachibana S., Tomomura S., Spicuzza M. J., Fournelle J. H. and Valley J. W. (2010) High precision SIMS oxygen three isotope study of chondrules in LL3 chondrites: role of ambient gas during chondrule formation. *Geochim. Cosmochim. Acta* **72**, 6610–6635.

Kohn M. J. (1999) Why most "dry" rocks should cool "wet". *Am. Mineral.* **84**, 570–580.

Kohn M. J., Valley J. W., Elsenheimer D. and Spicuzza M. (1993) Oxygen isotope zoning in garnet and staurolite: evidence for closed system mineral growth during regional metamorphism. *Am. Mineral.* **78**, 988–1001.

Kozdon R., Ushikubo T., Kita N. T. and Valley J. W. (2009) Intratest oxygen isotope variability in planktonic foraminifera: new insights from in situ measurement by ion microprobe. *Chem. Geol.* **258**, 327–337.

Labotka T. C., Cole D. R. and Riciputi L. R. (2000) Diffusion of C and O in calcite at 100 MPa. *Am. Mineral.* **85**, 488–494.

Labotka T. C., Cole D. R., Fayek M. J. and Chacko T. (2010) An experimental study of the diffusion of C and O in calcite in mixed CO_2–H_2O fluid. *Geochim. Cosmochim. Acta* **74**, A553 (abstr.).

Lackey J. S. and Valley J. W. (2004) Complex patterns of fluid flow during wollastonite formation in calcareous sandstones at Laurel Mountain, Mt. Morrison pendant, California. *Geol. Soc. Am. Bull.* **116**, 76–93.

Lancaster P. J., Fu B., Page F. Z., Kita N. T., Bickford M. E., Hill B. M., McLelland J. M. and Valley J. W. (2009) Genesis of metapelitic migmatite in the Adirondack Mts., New York. *J. Metamorph. Geol.* **27**, 41–54.

Lattanzi P., Rye D. M. and Rice J. M. (1980) Behavior of ^{13}C and ^{18}O in carbonates during contact metamorphism at Marysville, Montana: implications for isotope systematics in impure dolomitic limestones. *Am. J. Sci.* **280**, 890–906.

Lewis S., Holness M. and Graham C. M. (1998) Ion microprobe study of marble from Naxos, Greece: grain-scale fluid pathways and stable isotope equilibration during metamorphism. *Geology* **26**, 935–938.

Lyubetskaya T. and Ague J. J. (2009) Effect of metamorphic reactions on thermal evolution in collisional orogens. *J. Metamorph. Geol.* **27**, 579–600.

Mahon K. I. (1996) The new "York" regression: application of an improved statistical method to geochemistry. *Int. Geol. Rev.* **38**, 293–303.

Müller T., Baumgartner L. P., Foster, Jr., C. T. and Vennemann T. W. (2004) Metastable prograde mineral reactions in contact aureoles. *Geology* **32**, 821–824.

Müller T., Baumgartner L. P., Foster C. T. and Bowman J. R. (2009) Crystal size distribution of periclase in contact metamorphic dolomite marbles from the southern Adamello Massif, Italy. *J. Petrol.* **50**, 451–465.

Nabelek P. I. (1991) Stable isotope monitors. In *Contact Metamorphism*, vol. 26 (ed. D. M. Kerrick). *Rev. Mineral.* pp. 395–435.

Nabelek P. I. (2009) Numerical simulation of kinetically-controlled calc-silicate reactions and fluid flow with transient permeability around crystallizing plutons. *Am. J. Sci.* **309**, 517–548.

Page F. Z., Ushikubo T., Kita N. T., Riciputi L. R. and Valley J. W. (2007) High precision oxygen isotope analysis of picogram samples reveals 2-μm gradients and slow diffusion in zircon. *Am. Mineral.* **92**, 1772–1775.

Page F. Z., Kita N. T. and Valley J. W. (2010) Ion microprobe analysis of oxygen isotopes in garnets of complex chemistry. *Chem. Geol.* **270**, 9–19.

Penniston-Dorland S. C. and Ferry J. M. (2006) Development of spatial variations in reaction progress during regional metamorphism of micaceous carbonate rocks, northern New England. *Am. J. Sci.* **306**, 475–524.

Roselle G. T., Baumgartner L. P. and Chapman J. A. (1997) Nucleation-dominated crystallization of forsterite in the Ubehebe Peak contact aureole, California. *Geology* **25**, 823–826.

Roselle G. T., Baumgartner L. P. and Valley J. W. (1999) Stable isotope evidence for heterogeneous fluid infiltration at the Ubehebe Peak contact aureole, Death Valley National Park, California. *Am. J. Sci.* **299**, 93–138.

Rumble, D. III (1982) Stable isotope fractionation during metamorphic devolatilization reactions. In *Characterization of Metamorphism thorough Mineral Equilibria*, vol. 10 (ed. J. M. Ferry). *Rev. Mineral.* pp. 327–353.

Satish-Kumar M., Yoshida M., Wada H., Niisuma N. and Santosh M. (1998) Fluid flow along microfractures in calcite from a marble from East Antarctica: evidence from gigantic (21‰) oxygen isotopic zonation. *Geology* **26**, 251–254.

Sheppard S. M. F. and Schwarcz H. P. (1970) Fractionation of carbon and oxygen isotopes and magnesium between coexisting metamorphic calcite and dolomite. *Contrib. Mineral. Petrol.* **26**, 161–198.

Valley J. W. (1986) Stable isotope geochemistry of metamorphic rocks. In *Stable Isotopes in High Temperature Geological Processes*, vol. 16 (eds. J. W. Valley, H. P. Taylor Jr. and J. R. O'Neil). *Rev. Mineral.* pp. 445–490.

Valley J. W. (2001) Stable isotope thermometry at high temperatures. In *Stable Isotope Geochemistry*, vol. 43 (eds. J. W. Valley and D. R. Cole). *Rev. Mineral. Geochem.* pp. 365–414.

Valley J. W. and Graham C. M. (1991) Ion microprobe analysis of oxygen isotope ratios in metamorphic magnetite–diffusion reequilibration and implications for thermal history. *Contrib. Mineral. Petrol.* **109**, 38–52.

Valley J. W. and Graham C. M. (1993) Cryptic grain-scale heterogeneity of oxygen isotope ratios in metamorphic magnetite. *Science* **259**, 1729–1733.

Valley J. W. and Graham C. M. (1996) Ion microprobe analysis of oxygen isotope ratios in quartz from Skye granite: healed micro-cracks, fluid flow, and hydrothermal exchange. *Contrib. Mineral. Petrol.* **124**, 225–234.

Valley J. W. and Kita N. T. (2009) In situ oxygen isotope geochemistry by ion microprobe. In *Secondary Ion Mass Spectrometry in the Earth Sciences*, vol. 41 (ed. M. Fayek). *Mineral. Assoc. Canada Short Course*. pp. 19–63.

Van Haren J. L. M., Ague J. J. and Rye D. M. (1996) Oxygen isotope record of fluid infiltration and mass transfer during regional metamorphism of pelitic schist, south-central Connecticut, USA. *Geochim. Cosmochim. Acta* **60**, 3487–3504.

Wada H. (1988) Microscale isotopic zoning in calcite and graphite crystals. *Nature* **331**, 61–63.

Wada H., Ando T. and Suzuki M. (1998) The role of the grain boundary at chemical and isotopic fronts in marble during contact metamorphism. *Contrib. Mineral. Petrol.* **132**, 309–320.

Wing B. A. and Ferry J. M. (2007) Magnitude and geometry of reactive fluid flow from direct inversion of spatial patterns of geochemical alteration. *Am. J. Sci.* **307**, 793–832.

Wing B. A., Ferry J. M. and Rumble D. (2000) Controls on porosity development during contact metamorphism. *Geol. Soc. Am. Abs. Programs* **32**, A295 (abstr.).

Wing B. A., Ferry J. M. and Harrison T. M. (2003) Prograde destruction and formation of monazite and allanite during contact and regional metamorphism of pelites: petrology and geochronology. *Contrib. Mineral. Petrol.* **145**, 228–250.

Young E. D. and Rumble D. (1993) The origin of correlated variations in in-situ $^{18}O/^{16}O$ and elemental concentrations in metamorphic garnet from southeastern Vermont, USA. *Geochim. Cosmochim. Acta* **57**, 2585–2597.

Associate editor: James Farquhar